# Mechanisms of Interactions of the Nucleotide Cofactor with the RepA Protein of Plasmid RSF1010. Binding Dynamics Studied Using the Fluorescence Stopped-Flow Method

**ARTICLE** *in* BIOCHEMISTRY · SEPTEMBER 2009

Impact Factor: 3.02 · DOI: 10.1021/bi900940q · Source: PubMed

Published in final edited form as:
*Biochemistry*. 2009 November 10; 48(44): 10620–10636. doi:10.1021/bi900940q.

# Mechanisms of Interactions of the Nucleotide Cofactor with the RepA Protein of Plasmid RSF1010. Binding Dynamics Studied Using the Fluorescence Stopped-Flow Method†

**Iraida E. Andreeva**, **Anasuya Roychowdhury**, **Michal R. Szymanski**, **Maria J. Jezewska**, and **Wlodzimierz Bujalowski***
Department of Biochemistry and Molecular Biology, Department of Obstetrics and Gynecology, Sealy Center for Structural Biology, and Sealy Center for Cancer Cell Biology, The University of Texas Medical Branch at Galveston, 301 University Boulevard, Galveston, Texas 77555-1053

## Abstract

The dynamics of the nucleotide binding to a single, noninteracting nucleotide-binding site of the hexameric helicase RepA protein of plasmid RSF1010 has been examined, using the fluorescence stopped-flow method. The experiments have been performed with fluorescent analogues of ATP and ADP, TNP-ATP and TNP-ADP, respectively. In the presence of $Mg^{2+}$, the association of the cofactors proceeds as a sequential three-step process

$$\text{RepA hexamer} + \text{N} \underset{k_{-1}}{\overset{k_1}{\rightleftarrows}} (\text{H}-\text{N})_1 \underset{k_{-2}}{\overset{k_2}{\rightleftarrows}} (\text{H}-\text{N})_2 \underset{k_{-3}}{\overset{k_3}{\rightleftarrows}} (\text{H}-\text{N})_3$$

The sequential nature of the mechanism indicates the lack of significant conformational equilibria of the helicase prior to nucleotide binding. The major conformational change of the RepA helicase–nucleotide complex occurs in the formation of $(H–N)_2$, which is characterized by a very high value of the partial equilibrium constant and large positive changes in the apparent enthalpy and entropy. Strong stabilizing interactions between subunits of the RepA hexamer contribute to the observed dynamics and energetics of the internal transitions of the formed complexes. Magnesium cations mediate the efficient and fast conformational transitions of the protein, in a manner independent of the structure of the cofactor phosphate group. The ssDNA bound to the enzyme preferentially selects a single intermediate of the RepA–ATP analogue complex, $(H–N)_2$, while the DNA has no effect on the intermediates of the RepA–ADP complex. Allosteric interactions between the nucleotide- and DNA-binding site are established in the initial stages of formation of the complex. Moreover, in the presence of the single-stranded DNA, all the transitions in the nucleotide binding to the helicase become sensitive to the structure of the phosphate group of the cofactor.

The metabolic processes of DNA and RNA, such as replication, recombination, and translation, require that the duplex conformation of the nucleic acid be unwound to form a transiently metabolically active single-stranded intermediate (1–7). The unwinding reaction is catalyzed by a class of enzymes called helicases, and the process is fueled by the

†This work was supported by National Institutes of Health Grant GM46679 (to W.B.).



*To whom correspondence should be addressed: Department of Biochemistry and Molecular Biology, The University of Texas Medical Branch at Galveston, 301 University Blvd., Galveston, TX 77555-1053. Telephone: (409) 772-5634. Fax: (409) 772-1790. wbujalow@utmb.edu.

hydrolysis of nucleoside triphosphates (1–7). The replicative helicases are predominantly homohexamers built of six identical subunits (3–7). The RepA hexameric helicase is coded by broad host nonconjugative plasmid RSF1010, which confers bacterial resistance to sulfonamides, and streptomycin (8–11). The RepA enzyme is the DNA replicative helicase, which is essential for the RFS1010 plasmid replication and unwinds the dsDNA[1] in a 5′ → 3′ direction (10,11). The molecular mass of the RepA monomer is 29896 Da; i.e., it is one of the smallest known helicases. The crystal structure of the RepA hexamer has been determined at 2.5 Å resolution (11). The diameter of a single hexamer is ~115Å, while the diameter of the central cross channel of the ringlike structure of the enzyme is only ~17Å. What distinguishes the RepA hexamer from other hexameric helicases is its unusual stability, which does not require any additional interactions with the nucleic acid and/or nucleotides (10–14). In this context, the RepA hexamer resembles the *Escherichia coli* replicative helicase, DnaB protein, whose hexameric structure stability requires only $Mg^{2+}$ cations (15,16). Several well-known helicases form hexameric ringlike structures, which are stabilized by nucleotides and/or DNA binding (17–20).

Although the unwinding of the duplex nucleic acid and mechanical translocation along the single-stranded (ss) nucleic acid lattice require binding and hydrolysis of nucleoside cofactors (NTPs and NDPs) by a helicase, the mechanism of how the binding or hydrolysis of cofactors regulates the activity of the enzyme is still not completely understood for any helicase, particularly, at the molecular level. At saturation, the RepA hexamer binds six nucleotides, indicating that each subunit of the helicase can engage in interactions with the cofactor (13,14). The nucleotide macroscopic affinity decreases with an increasing degree of binding, resulting from negative cooperative interactions between the binding sites. Thus, the nucleotide-binding sites of the RepA hexamer are initially independent, and the negative cooperative interactions reflect interactions between the sites saturated with the cofactor (13,14).

Recent analytical ultracentrifugation and dynamic light scattering studies revealed that the global conformation of the RepA hexamer is modulated by a specific number of bound nucleotides (21). The enzyme exists in at least four conformational states, occurring sequentially as a function of the number of bound cofactors. These conformational states are different for the nucleoside diphosphate, as compared to the nucleoside triphosphate. Modulation of the global structure is separated into two phases, different for complexes with up to three bound nucleotides, from the effect observed with all binding sites saturated with the cofactor. This heterogeneity indicates different functional roles of the two modulation processes. The control of helicase–ssDNA interactions by the cofactors results from binding the first one and/or two nucleotide molecules (21). Not only is the ssDNA affinity of the enzyme dramatically higher, but the site size of the tertiary RepA–ssDNA–nucleotide complex is increased.

Quantitative information about the interactions of the RepA helicase with nucleotide cofactors is a necessary prerequisite for the formulation of a model of the activity of the enzyme. Although equilibrium studies shed some light on the intricate nature of the nucleotide–RepA interactions, nothing is known about the dynamics of binding of the cofactor to the RepA hexamer, internal energetics among the intermediates of the reaction, or the functional roles of the intermediates. Moreover, the functional and structural homology between the RepA and DnaB hexamers makes RepA protein an excellent system for comparative studies and of paramount importance for understanding the general aspects of the hexameric helicase activities. The RepA helicase is essential for RSF1010 plasmid

[1]Abbreviations: TNP-ATP, 2′(3′)-*O*-(2,4,6-trinitrophenyl)adenosine triphosphate; TNP-ADP, 2′(3′)-*O*-(2,4,6-trinitrophenyl)adenosine 5′-diphosphate; NTP, nucleoside triphosphate; DTT, dithiothreitol; dsDNA, double-stranded DNA; ssDNA, single-stranded DNA.

replication, which suggests that the protein is involved in specific mechanisms during DNA replication that are not yet understood. The essential role of the helicase in replication of RSF1010, a ubiquitous plasmid, conferring resistance to antibiotics, provides an opportunity to examine molecular aspects of such resistance (8–10).

In this work, we address the kinetics of nucleotide binding to the single, noninteracting site of the RepA hexamer, using the fluorescent nucleotide analogues (13,14,22–27). The association of the cofactors with the single binding site on the RepA hexamer proceeds through a minimum three-step sequential mechanism. The major conformational change of the RepA helicase–nucleotide complex occurs in the formation of the second intermediate, $(H–N)_2$. Moreover, $Mg^{2+}$ cations affect the efficiency and dynamics of the conformational transitions of the protein. The ssDNA preferentially selects a single intermediate of the RepA–ATP analogue complex. The allosteric interactions between the nucleotide- and DNA-binding sites are already established in the initial stages of formation of the complex, with the conformational transitions of the complex becoming sensitive to the structure of the cofactor phosphate group.

## MATERIALS AND METHODS

### Reagents and Buffers

All solutions were made with distilled and deionized >18 MΩ (Milli-Q Plus) water. All chemicals were reagent grade. Buffer T5 consists of 50mM Tris adjusted to pH7.6 with HCl, 10 mM NaCl, and 10%glycerol (13,14). The temperature and $MgCl_2$ concentrations in the buffer are given in the text.

### RepA Helicase of Plasmid RSF1010

Isolation and purification of the protein were performed, with slight modifications, as previously described (12–14,21). The protein concentration was spectrophotometrically determined using an extinction coefficient $\varepsilon_{280}$ of $1.656 \times 10^5$ $cm^{-1}M^{-1}$, obtained with the approach based on Edelhoch's method (22,23).

### Nucleotides

TNP-ATP and TNP-ADP were from Molecular Probes (Eugene, OR) (13,24–30).

### Steady-State Fluorescence Measurements

All steady-state fluorescence titrations were performed using the Fluorolog F-11 spectrofluorometer (Jobin Yvon) (13,14,24–29,31–35). The binding was followed by monitoring the fluorescence of the TNP analogues ($\lambda_{ex}$ = 410 nm, and $\lambda_{em}$ = 560 nm). Computer fits were performed using Mathematica (Wolfram) and Kaleida-Graph (Synergy Software, Reading, PA). All titration points were corrected for dilution and inner filter effects using the following formula (31–35):

$$F_{icor}=(F_i - B_i)\left(\frac{V_i}{V_o}\right) \times 10^{0.5bA_{i,\lambda ex}} \quad (1)$$

where $F_{icor}$ is the corrected value of the fluorescence intensity at a given point of titration, $F_i$ is the experimentally measured fluorescence intensity, $B_i$ is the background, $V_i$ is the volume of the sample at a given titration point, $V_o$ is the initial volume of the sample, $b$ is the total length of the optical path of the sample in centimeters, and $A_{i\lambda_{ex}}$ is the absorbance of the sample at the excitation wavelength (24–29,31–35). The relative fluorescence increase,

$\Delta F_{obs}$, upon binding equals $(F_{icor} - F_o)/F_o$, where $F_o$ is the initial value of the fluorescence of the sample.

## Stopped-Flow Kinetics

All fluorescence stopped-flow kinetic experiments were performed using the SX.18MV stopped-flow instrument (Applied Photophysics Ltd., Leatherhead, U.K.). The reactions were monitored using the total fluorescence of the TNP analogues with a $\lambda_{ex}$ of 408 nm and the emission observed through a GG500 cutoff filter (Schott), with the excitation monochromator slits at 1mm (band-pass at ~4.5 nm). The sample was excited with vertically polarized light, and the time-development of the function

$$F(t)=I_{VV}(t)+2GI_{VH}(t) \quad (2)$$

was monitored, where $I_{VV}$ is the fluorescence intensity and the first and second subscripts refer to vertical (V) polarization of the excitation and vertical (V) or horizontal (H) polarization of the emitted light. The factor $G = I_{HV}/I_{HH}$ corrects for the different sensitivity of the emission monochromator for vertically and horizontally polarized light (22–37). The kinetic curves were fitted to extract the relaxation times and the amplitudes using nonlinear least-squares software provided by the manufacturer, with the exponential function defined as

$$F(t)=F(\infty)+\sum_{i=1}^{n} A_i \exp(-\lambda_i t) \quad (3)$$

where $F(t)$ is the fluorescence intensity at time $t$, $F(\infty)$ is the fluorescence intensity at time $\infty$, $A_i$ is the amplitude corresponding to the $i$th relaxation process, $\lambda_i$ is the time constant (reciprocal relaxation time) characterizing the $i$th relaxation process, and $n$ is the number of relaxation processes. All analyses of the data were performed using Mathematica (Wolfram, Urbana, IL) and Kaleida Graph (Synergy Software).

## Analysis of Stopped-Flow Kinetic Data

Analyses of the stopped-flow kinetic data have been performed using the matrix projection operator technique (35,38–45). This approach is particularly useful in analyzing the amplitudes of the studied reactions and has been extensively described by us (35,38–45).

## Analytical Ultracentrifugation Measurements

Sedimentation velocity experiments were performed with an Optima XL-A analytical ultracentrifuge (Beckman Inc., Palo Alto, CA) using double-sector charcoal-filled 12 mm centerpieces, as we previously described (12,15,21,26). Sedimentation velocity scans were collected at the absorption band of the RepA protein at 280 nm, or at the absorption band of the TNP moiety at 410 nm. Time-derivative analysis of the scans was performed with the software supplied by the manufacturer. The values of sedimentation coefficients were corrected to $s_{20,w}$ for solvent viscosity and temperature to standard conditions (12,15,21,26).

## RESULTS

### Binding of the Fluorescent Nucleotide Analogues, TNP-ADP and TNP-ATP, to a Single, Noninteracting Site of the RepA Hexamer in the Presence and Absence of Magnesium Cations

Binding of six nucleotide cofactors to the RepA hexamer is a biphasic process, containing a weak and a strong binding phase, resulting from the negative cooperativie interactions limited to two adjacent subunits (13,14). In other words, the nucleotide-binding sites of the enzyme are initially independent and the association of any of the first three cofactor molecules predominantly occurs at three noninteracting sites (13,14,35). Moreover, there is no detectable hydrolysis of TNP-ATP by the RepA helicase on the time scale of the equilibrium experiment, and the cofactor efficiently competes with unmodified nucleotides for the same binding sites (13,14). Such behavior of the system allows us to directly address the energetics of the nucleotide binding to a single, noninteracting nucleotide-binding site of the enzyme, as well as to obtain information about the environment surrounding the cofactor in the binding site (45).

Fluorescence titrations of TNP-ATP with the RepA helicase in buffer T5, containing 5 mM $MgCl_2$, at two different temperatures, 10 and 20 °C, are shown in Figure 1a. The applied low concentration of the cofactor ($3 \times 10^{-7}$ M) ensures that only the association with a single binding site is observed (13, 14, 35). Saturation of the cofactor with the helicase induces a large, ~10.5-fold, increase in analogue fluorescence. Because the TNP fluorescence is strongly dependent upon the polarity of the environment, the data indicate that the cofactor is placed in a strongly hydrophobic environment in the binding site (see below) (25). The solid lines in Figure 1a are nonlinear least-squares fits using the single-site binding isotherm, defined as

$$\Delta F = \frac{\Delta F_{\max} K_{ov} [\mathrm{RepA}]_F}{1 + K_{ov} [\mathrm{RepA}]_F} \quad (4)$$

where $K_{ov}$ is the TNP-ATP intrinsic binding constant, $\Delta F_{max}$ is the maximum fluorescence increase for the nucleotide saturated with the enzyme, and $[RepA]_F$ is the free concentration of the RepA helicase expressed as the concentration of the protomers. The fits provide an excellent description of the experimental curves. The obtained values are as follows: $K_{ov}$ = $(2.1 \pm 0.4) \times 10^6$ $M^{-1}$ and $\Delta F_{max}$ = 10.6 ± 0.3 for the titration at 10 °C, and $K_{ov}$ = $(2.0 \pm 0.4) \times 10^6$ $M^{-1}$ and $\Delta F_{max}$ = 8.6 ± 0.3 for the titration at 20 °C (Table 1). Thus, the increase in temperature considerably affects the observed maximum fluorescence increase for the cofactor in the binding site. However, the intrinsic binding constant is, within experimental accuracy, unaffected by temperature, indicating the overall enthalpy change ($\Delta H_T \approx 0$). Moreover, the values of the binding constants are the same as those obtained using the protein fluorescence to monitor the interactions and analyzing the entire binding isotherm with the statistical thermodynamic model for the protein hexamer. This agreement between independent sets of data indicates that indeed binding to a single site is observed (Table 1) (13,14).

Analogous fluorescence titrations of TNP-ADP with the RepA helicase are shown in Figure 1b. The solid lines are nonlinear least-squares fits using the single-site binding isotherm (eq 4), which provide the following values: $K_{ov}$=$(8 \pm 1.6) \times 10^6$ $M^{-1}$ and $\Delta F_{max}$=5.1± 0.3 for the titration at 10 °C, and $K_{ov}$= $(8 \pm 1.6) \times 10^6$ $M^{-1}$ and $\Delta F_{max}$ = 5.0 ± 0.3 for the titration at 20 °C (Table 1) (13, 14). The lack of a detectable temperature effect on the observed binding process indicates that, similar to the ATP analogue, the overall enthalpy of the process is

$\Delta H_D \approx 0$. Moreover, the change in temperature does not affect $\Delta F_{max}$, indicating that, unlike TNP-ATP, the ADP analogue experiences an unchanged surrounding in the binding site at different temperatures. Nevertheless, the observed $\Delta F_{max}$ is significantly smaller than that observed for TNP-ATP (Table 1). These data provide the first indication that the location and/or structure of the ADP analogue, in the nucleotide-binding site of the RepA helicase, are different from the ATP analogue (13, 14, 21) (see below).

Magnesium has a profound effect on the nucleotide cofactor binding to the RepA hexamer (14). In the absence of $Mg^{2+}$, the affinities of both ATP and ADP analogues are significantly lower than those observed in the presence of magnesium (14). Fluorescence titrations of TNP-ATP with the RepA helicase, in the absence of $Mg^{2+}$, at two different temperatures, 10 and 20 °C, are shown in Figure 1c. The values of the binding constants are lower by a factor of ~4, as compared to the corresponding values in the presence of magnesium (Table 2). As observed in the presence of $Mg^{2+}$, the intrinsic binding constant is, within experimental accuracy, unaffected by the temperature, indicating that the overall enthalpy change, $\Delta H_T$, is ~0 (Table 2). Also, in the absence of magnesium, the temperature has little effect on the maximum relative fluorescence increase of TNP-ATP upon binding to the RepA helicase (Figure 1c and Table 2).

Fluorescence titrations of the ADP analogue TNP-ADP with the RepA helicase, at two different temperatures and in the absence of magnesium, are shown in Figure 1d. The binding constants are diminished by more than 1 order of magnitude, significantly more than observed for TNP-ATP, and, within experimental accuracy, are unaffected by temperature (Table 2). Nevertheless, the maximum relative fluorescence increase for TNP-ADP upon binding to the RepA helicase is still considerably smaller than that observed for the ATP analogue and is strongly affected by temperature (Table 2). Thus, the absence of magnesium has a more pronounced effect not only on the intrinsic affinity of the ADP analogue but also on the cofactor environment in the nucleotide-binding site, providing an additional indication that the structure of the nucleotide-binding site of the RepA helicase complex with the ADP analogue is different from the structure of the complex with TNP-ATP (see above) (14).

## Kinetics of the ATP Analogue TNP-ATP Binding to a Single, Noninteracting Site of the RepA Helicase in the Presence of Magnesium

The dynamics of the ATP and ADP analogue binding to the noninteracting nucleotide-binding site of the RepA helicase has been addressed using the fluorescence stopped-flow technique (35,38–46). The kinetic measurements have been performed under pseudo-first-order conditions by mixing the nucleotide with a large excess of the RepA helicase (35,38–46). The fluorescence stopped-flow kinetic traces, after $5 \times 10^{-7}$ M TNP-ATP had been mixed with different concentrations of the RepA helicase in buffer T5 (10 °C), containing 5 mM $MgCl_2$, are shown in Figure 2. The reference trace, obtained after the cofactor had been mixed with only the buffer, at the same final concentration of the nucleotide as with the protein, is also included in Figure 2. All traces were recorded at two time bases. The observed kinetics is complex, indicating the presence of multiple steps. At lower enzyme concentrations, there is a monotonous increase in cofactor fluorescence. However, at higher concentrations of the helicase, the initial large increase in the nucleotide fluorescence precedes the slower process, which is characterized by the lower fluorescence intensity. Moreover, there is also a significant part of the observed increase in fluorescence emission, which is beyond the time resolution of the stopped-flow measurement. Thus, the two identified relaxation processes are preceded by another fast step (35,40,47–49). The solid lines in Figure 2 are nonlinear least-squares fits of the experimental curves, which require the single-exponential function at lower enzyme concentrations and the double-exponential function in the high-concentraton range of the helicase (eq 3). The included deviations of the

experimental curve from the fit, recorderd at a RepA concentration of $9 \times 10^{-5}$ M (protomer), indicate that only the double-exponential function provides an adequate description of the experimentally observed kinetic traces. A higher number of exponents does not significantly improve the statistics of the fit (data not shown). Therefore, the association of TNP-ATP with the RepA helicase requires at least three steps, which includes the fast, unresolved step and two identified relaxation processes (35,40,47–49).

The dependence of the reciprocal relaxation times, $1/\tau_2$ and $1/\tau_3$, characterizing the observed relaxation steps for the ATP analogue binding to the noninteracting nucleotide-binding site of the RepA helicase, as a function of the total RepA helicase concentration, $[\mathrm{RepA}]_T$ (protomer), is shown in Figure 3a,b. In the lower-enzyme concentration range, the reciprocal relaxation times have similar values, indicating a coupling of both relaxation processes; i.e., their equilibrations are mutually dependent (35, 50, 51). However, the coupling becomes weaker with an increase in protein concentration. The larger reciprocal relaxation time, $1/\tau_2$, increases with an increase in $[\mathrm{RepA}]_T$ and shows only slightly marked hyperbolic character (35, 50, 51). These data and the presence of the very fast, unresolved process (Figure 2) indicate that $1/\tau_2$ describes the intramolecular transition of the formed complex (35, 38–46, 50, 51). On the other hand, $1/\tau_3$ shows a clear hyperbolic dependence upon $[\mathrm{RepA}]_T$, indicating that it represents the internal transition of the complex. The simplest, minimum mechanism that can account for the observed dependence of the reciprocal relaxation times on enzyme concentration and the presence of the fast, unresolved step is a three-step, sequential binding process, in which bimolecular association is followed by two isomerization steps, as described by

$$\mathrm{RepA\ hexamer} + \mathrm{N} \underset{k_{-1}}{\overset{k_1}{\rightleftarrows}} (\mathrm{H-N})_1 \underset{k_{-2}}{\overset{k_2}{\rightleftarrows}} (\mathrm{H-N})_2 \underset{k_{-3}}{\overset{k_3}{\rightleftarrows}} (\mathrm{H-N})_3 \tag{5}$$

To extract the rate constants from the relaxation time data, we utilize the fact that the value of the overall binding constant ($K_{ov} \approx 2.1 \times 10^6\ \mathrm{M}^{-1}$) has been independently obtained under the same solution conditions by the equilibrium fluorescence titration method (Figure 1a). The overall binding constant, $K_{ov}$, is related to the partial equilibrium steps in eq 5, as

$$K_{ov} = K_1(1 + K_2 + K_2K_3) \tag{6}$$

The partial equilibrium constants, $K_1$, $K_2$, and $K_3$, for each step of the reaction (eq 5), are as follows: $K_1 = k_1/k_{-1}$, $K_2 = k_2/k_{-2}$, and $K_3 = k_3/k_{-3}$. Expression 6 reduces the number of fitting parameters by one (see below). Even though we cannot determine the value of the reciprocal relaxation time, $1/\tau_1$, for the first fast relaxation process, we can determine its amplitude, $A_1$, as (35,47–49)

$$A_1 = A_T - A_2 - A_3 \tag{7}$$

where $A_T$ is the experimentally observed total amplitude of the kinetic trace at a given total concentration of the RepA helicase (35,47–49). The dependence of the individual amplitudes, $A_1$, $A_2$, and $A_3$, of all three observed relaxation processes on the total concentration of RepA protein (protomer) is shown in Figure 3c. The individual amplitudes are normalized, i.e., expressed as fractions of the total amplitude, $A_i/\Sigma A_i$. At the low enzyme concentrations, the total observed amplitude, $A_T$, is dominated by $A_3$ while amplitude $A_1$ of

the fast process is barely detectable. Amplitude $A_3$ sharply decreases with the increase in $[RepA]_T$ and assumes negative values in the high protein concentration range. The positive amplitude, $A_3$, appears at higher protein concentrations, where it dominates the relaxation process. With an increase in $[RepA]_T$, the values of $A_3$ gradually decrease while the values of the amplitude of the fast process, $A_1$, are positive and steadily increase in the high-protein concentration range. Such behavior of the individual amplitudes is in complete agreement with the proposed kinetic mechanism (eq 5) based on the behavior of the relaxation times (35,47–50).

With determined individual amplitudes, we can address the molar fluorescence intensities characterizing each intermediate of the reaction, using the matrix projection operator approach (35,47–49). In this analysis, we use the maximum, fractional increase in cofactor fluorescence ($\Delta F_{max} \approx 10.6$) obtained in independent equilibrium titrations (Figure 1a). The values of $\Delta F_{max}$ can be analytically expressed as

$$\Delta F_{max} = \frac{\Delta F_1 + K_2 \Delta F_2 + K_2 K_3 \Delta F_3}{1 + K_2 + K_2 K_3} \quad (8)$$

where $\Delta F_1$, $\Delta F_2$, and$\Delta F_3$ are fractional fluorescence intensities of the corresponding intermediates in the association reaction of TNP-ATP with the RepA helicase, relative to the fluorescence of the free nucleotide, $F_0$, i.e., $\Delta F_i = (F_i - F_0)/F_0$. The value of $F_0$ can be taken to be 1. Expression 8 provides an additional relationship among the fluorescence parameters, reducing the number of fitted spectroscopic parameters by one. Moreover, the value of $\Delta F_{max}$ plays the role of a scaling factor in the analysis (35,38–49).

The solid lines in panels a–c of Figure 3 are nonlinear least-squares fits of the experimentally determined reciprocal relaxation times and the fractional individual amplitudes of the reaction (eq 5), using a single set of binding and spectroscopic parameters. The following strategy is used in the numerical analysis (35,38–49). First, the nonlinear least-squares fitting of the individual relaxation times and then simultaneous fitting of all three relaxation times are performed. Subsequently, the individual amplitudes are fitted, using the rate constants obtained from the relaxation time analysis, or allowing these rate constants to float between ±10% of the determined values. Finally, global fitting, with the simultaneous analysis of all relaxation times and individual amplitudes, refines the obtained parameters. The obtained kinetic and spectroscopic parameters for binding of TNP-ATP to the noninteracting nucleotide-binding site of the RepA helicase are included in Table 1.

The value of the partial equilibrium constants, $K_1$, which describes the formation of the intermediate, $(H–N)_1$, in eq 5, is ~$4.8 \times 10^3$ $M^{-1}$ (Table 1). Thus, the formation of the first intermediate makes a dominant contribution to the free energy of ATP analogue binding. At 10 °C, the next two steps of the reaction increase the overall affinity. However, the value of $K_2$, which characterizes the $(H–N)_1 \leftrightarrow (H–N)_2$ transition, is ~118, i.e., the first isomerization step in ATP analogue binding provides a dramatic increase in the free energy of binding. This is very different from the analogous *E. coli* DnaB helicase where the first isomerization step in ATP analogue binding is characterized by a $K_2$ of ≈1.3 (41) (see Discussion). On the other hand, the values of $K_3$, which describes the $(H–N)_2 \leftrightarrow (H–N)_3$ transition, is ~2.6; i.e., it makes only a modest contribution to the overall affinity (Table 1). As observed for the partial equilibria, the dynamics of the second, $(H–N)_1 \leftrightarrow (H–N)_2$, and third, $(H–N)_2 \leftrightarrow (H–N)_3$, steps of the reaction are also very different. The value of the forward rate constant ($k_2 \approx 59$) is more than 1 order of magnitude larger than the $k_3$ of ≈3.9. Conversely, the $k_{-2}$ value of ≈0.5 is, by a factor of ~3, lower than the $k_{-3}$ of ≈1.5 (Table 1).

The enzyme locks itself quickly and very efficiently in the $(H–N)_2$ state, which slowly transforms into the $(H–N)_3$ intermediate (see Discussion). The bound TNP-ATP experiences the largest, ~16-fold increase in its fluorescence emission intensity, as compared to the free cofactor in the first intermediate, $(H–N)_1$. In the subsequent intermediates, $(H–N)_2$ and $(H–N)_3$, the fluorescence intensity of the bound nucleotide is high, although lower than in $(H–N)_1$ (Table 1) (see Discussion).

## Kinetics of the ADP Analogue TNP-ADP Binding to a Single, Noninteracting Site of the RepA Helicase in the Presence of Magnesium

The kinetic mechanism of binding of TNP-ADP to the RepA helicase has been analogously examined as described for TNP-ATP above (38–49). At higher enzyme concentrations, the kinetic traces required a double-exponential function (eq 3) to adequately represent the experimental curves (data not shown). Moreover, a significant part of the increase in analogue fluorescence occurs in the very short time range beyond the time resolution of the stopped-flow measurement. Therefore, the association of TNP-ADP with the RepA helicase consists of at least three steps, the fast, unresolved step and two resolved relaxation processes (38–51). The dependencies of the reciprocal relaxation times and the amplitudes of all three observed relaxation processes on the total RepA helicase concentration, $[RepA]_T$ (protomer), indicate that the simplest minimum mechanism that can account for these data is a three-step, sequential binding process as described by eq 5 (data not shown) (38–51). The obtained kinetic and spectroscopic parameters for the binding of TNP-ADP to the RepA helicase are included in Table 1.

Under the examined solution conditions, the formation of the first intermediate, $(H–N)_1$, makes a dominant contribution to the free energy of ADP analogue binding (Table 1). The value of the partial equilibrium constants ($K_1 \approx 1.0 \times 10^4\ M^{-1}$) is larger than that observed for TNP-ATP. The value of $K_2$, which characterizes the $(H–N)_1 \leftrightarrow (H–N)_2$ transition, is ~200; i.e., the first isomerization step dramatically increases the overall affinity. The value of $K_3$ is ~3.0; i.e., it makes only a modest contribution to the overall affinity (Table 1). The differences in the dynamics of the second, $(H–N)_1 \leftrightarrow (H–N)_2$, and third, $(H–N)_2 \leftrightarrow (H–N)_3$, steps of the reaction are also similar to the dynamics of the corresponding steps observed for the ATP analogue (Table 1). Nevertheless, in spite of similar dynamics and energetics, significant differences between the ATP and ADP analogue occur in the values of the molar fluorescence intensities of individual intermediates (Table 1) (35,38–49). The bound TNP-ADP experiences the largest, ~9-fold increase in its fluorescence emission intensity, as compared to the free cofactor in the first intermediate, $(H–N)_1$. However, this value is by a factor of ~1.8 lower than the corresponding parameter observed for TNP-ATP, indicating a very different surrounding of the bound ADP analogue in the binding site, as compared to the ATP analogue (see Discussion). Similarly, the values of the molar fluorescence intensities of the bound TNP-ADP are significantly lower than those observed for TNP-ATP in subsequent intermediates, $(H–N)_2$ and $(H–N)_3$ (Table 1).

## Effect of Magnesium on the Binding Dynamics of the ATP and ADP Analogues to the Single, Noninteracting Nucleotide-Binding Site of the RepA Helicase

Analogous kinetic stopped-flow studies of TNP-ATP and TNP-ADP, as described above, have been performed in the absence of magnesium. The general aspects of the kinetic mechanism of the binding of the ADP analogue to the RepA helicase are not affected by the absence of magnesium; i.e., the association process is a three-step sequential reaction as defined by eq 5 (data not shown). Nevertheless, the dynamics and internal energetics of the intermediates of the reaction are dramatically different compared to the behavior of the system in the presence of $Mg^{2+}$ (see below). On the other hand, at 10 °C, the binding of TNP-ATP becomes a more complex process. Besides the fast, unresolved step, the kinetic

traces require a triple-exponential function (eq 3) to adequately represent the experimental curves (data not shown).

The dependencies of the reciprocal relaxation times, $1/\tau_2$, $1/\tau_3$, and $1/\tau_4$, on total RepA helicase concentration, $[RepA]_T$ (protomer), for the TNP-ATP association reaction in the absence of $Mg^{2+}$, are shown in panels a–c of Figure 4, respectively. The values of $1/\tau_2$, $1/\tau_3$, and $1/\tau_4$ differ by more than 1 order of magnitude through the entire examined enzyme concentration range, indicating that the observed relaxation processes are now close to "decoupled" ones; i.e., they equilibrate independently from each other (35,50,51). Moreover, all three reciprocal relaxation times do not show much dependence upon $[RepA]_T$, indicating that they describe intramolecular transitions of the complex (35,50,51). The simplest mechanism that can account for the observed dependence of the reciprocal relaxation times on enzyme concentration and the presence of the fast, unresolved step is a four-step, sequential binding process

$$\text{RepA hexamer} + \text{N} \underset{k_{-1}}{\overset{k_1}{\rightleftarrows}} (\text{H}-\text{N})_1 \underset{k_{-2}}{\overset{k_2}{\rightleftarrows}} (\text{H}-\text{N})_2 \underset{k_{-3}}{\overset{k_3}{\rightleftarrows}} (\text{H}-\text{N})_3 \underset{k_{-4}}{\overset{k_4}{\rightleftarrows}} (\text{H}-\text{N})_4 \quad (9)$$

The dependence of normalized individual amplitudes $A_1$, $A_2$, $A_3$, and $A_4$ on the logarithm of the total concentration of the RepA helicase (protomer) is shown in Figure 4d. The observed behavior of the individual amplitudes is very different from the behavior observed in the presence of magnesium (Figure 3c), indicating a profound change in the internal energetics and dynamics of the association reaction (see below). $A_1$ is large and dominates the relaxation process. The values of $A_2$ are low and show little dependence on $[RepA]_T$. The values of $A_3$ and $A_4$ are also low and gradually decrease with an increase in $[RepA]_T$, although none of the amplitudes becomes negative in the high-enzyme concentration range. The obtained kinetic and spectroscopic parameters for binding of TNP-ATP and TNP-ADP to the RepA helicase, in the absence of $Mg^{2+}$, are included in Table 2.

The dramatic effect of magnesium on the overall equilibrium binding process (Figure 1b,c) of the nucleotide cofactors to the RepA helicase is clearly reflected in the dynamic behavior of the cofactor binding (Table 2). The values of partial equilibrium constant $K_1$ are higher by factors of ~6 and ~20, in the absence of $Mg^{2+}$, for the ADP and ATP analogue, respectively. Thus, the very binding step of the nucleotide cofactors is more favorable in the absence of magnesium. However, the most surprising is the staggering decrease in the value of the partial equilibrium constant, $K_2$, which decreases by approximately 2–3 orders of magnitude in the absence of $Mg^{2+}$ cations (Tables 1 and 2). The decrease in $K_2$ is predominantly responsible for the decrease in the overall affinity of the nucleotide cofactors in the absence of $Mg^{2+}$ (Figure 1c,d). In the case of the ADP analogue, this decrease is partially compensated by an increase in the value of $K_3$, while for the ATP analogue, $K_3$ remains unchanged in the absence of magnesium. Recall that in the case of TNP-ATP, an additional process, characterized by a partial equilibrium constant ($K_4 \approx 3.5$), becomes detectable in the absence of $Mg^{2+}$.

The changes in the internal energetics of the association reaction of both nucleotide cofactors are reflected in the large changes in the dynamics of particular reaction steps (Table 2). The forward rate constant, $k_2$, decreases from 59 and 30 $s^{-1}$ to 7 and 1 $s^{-1}$, for the ATP and ADP analogue, respectively. On the other hand, the corresponding values of $k_{-2}$ increase from ~0.5 and ~0.15 $s^{-1}$ to ~28 and ~7 $s^{-1}$, for TNP-ATP and TNP-ADP, respectively. In other words, the formation of intermediate $(H–N)_2$ is slower, but the rates of returning back to intermediate $(H–N)_1$ are ~2 orders of magnitude faster. In the case of the

ADP analogue, the partial equilibrium constant, $K_3$, is increased predominantly due to the much lower value of $k_{-3}$ (≈0.05 $s^{-1}$), as compared to the $k_{-3}$ of ≈3.3 $s^{-1}$, determined in the presence of magnesium (Tables 1 and 2). For the ATP analogue, the dynamics of the $(H–N)_2 \leftrightarrow (H–N)_3$ transition is much less affected by the absence of $Mg^{2+}$ and is followed by an additional slow process (Tables 1 and 2).

The absence of magnesium is also reflected in the changes in the molar fluorescence intensities of different intermediates of the association reaction of both cofactors, indicating significant differences in the conformational transitions of the examined complexes, as compared to the analogous transitions observed in the presence of magnesium (Tables 1 and 2). The increases in the fluorescence intensity of the cofactors in the first intermediate, $(H–N)_1$, are lower than those observed in the presence of magnesium (Table 1). The largest increase in cofactor fluorescence intensity occurs in the second intermediate, $(H–N)_2$, where the relative fluorescence intensities reach values of ~23 and ~12 for the ATP and ADP analogue, respectively, as compared to the corresponding values of ~14 and ~6, in the presence of magnesium. On the other hand, the values of the fluorescence intensities of the ATP and ADP analogues in $(H–N)_3$ are similar to the values determined in the presence of $Mg^{2+}$ (Tables 1 and 2). Also, the ATP analogue does not experience significant changes in the environment of the binding site in the fourth intermediate, $(H–N)_4$ (Table 2) (see Discussion).

## Effect of Temperature on the Dynamics of Binding of the ATP and ADP Analogues to the Single Noninteracting Nucleotide-Binding Site of the RepA Helicase in the Presence and Absence of Magnesium

To further address the nature of different intermediates in the binding of the ATP and ADP analogues to the RepA helicase, we examined the effect of temperature on the dynamics of the reactions. The stopped-flow studies were analogously conducted at 20 °C in the presence and absence of magnesium, as described above (data not shown). The obtained kinetic and spectroscopic parameters for all examined complexes are included in Tables 1 and 2. In general, the temperature increase from 10 to 20 °C does not affect the major features of the observed kinetic mechanism, which is the three-step sequential process (eq 5). The additional process, seen at 10 °C in the binding of TNP-ATP, is not detectable at 20 °C. However, the effect of temperature on the internal equilibria differs among the reaction intermediates and is different in the presence and absence of $Mg^{2+}$ cations.

In the presence of magnesium, the values of the partial equilibrium constant, $K_1$, decrease with the increase in temperature for both ATP and ADP analogues (Table 1). On the other hand, the values of $K_2$ increase with the increase in temperature for both cofactors, mainly due to the increase in the values of the forward rate constants, $k_2$, at a higher temperature. In contrast, the partial equilibrium constant, $K_3$, increases with temperature only for the ATP analogue; for TNP-ADP, it is unaffected by temperature (Table 1). A temperature increase has little effect on the relative fluorescence intensities of the intermediates of the reaction for both ATP and ADP analogues, which remain similar to the corresponding values obtained at 10 °C (Table 1). In the absence of $Mg^{2+}$, the partial equilibrium constant, $K_1$, is lower at a higher temperature for TNP-ADP binding, but it is unaffected by temperature in the case of TNP-ATP (Table 2). Nevertheless, the values of $K_2$ are very strongly increased at a higher temperature for both cofactors, while the values of $K_3$ are only modestly affected by the increased temperature (Table 2). Also, the increase in temperature strongly diminishes the relative fluorescence intensity of the second intermediate, $(H–N)_2$, for both ATP and ADP (Table 2).

The temperature dependence of the partial equilibrium constant, $K_i$, for each *i*th transition in the binding of the nucleotide cofactor to the RepA helicase is described by the van't Hoff

equation [$\partial \ln K/(\partial 1/T) = -\Delta H_i(1/T - 1/T_R)$] (52). $T_R$ is the reference temperature, taken as the lowest experimentally studied temperature, i.e., 10 °C, and $\Delta H_i$ is the enthalpy change accompanying the *i*th transition. The obtained values of the thermodynamic function, $\Delta H_i$ and $\Delta S_i$, characterizing the partial equilibria among the intermediates of the association reaction of TNP-ATP and TNP-ADP with the single, noninteracting nucleotide-binding site of the RepA helicase, are included in Table 3. The errors in the determined parameters are intrinsically large. Nevertheless, the observed differences are larger than the errors and provide important insight about the nature of the observed transitions.

In the presence of magnesium, the first binding step, H + N↔ $(H–N)_1$, is characterized by significant negative enthalpy changes and small entropy changes, suggesting a similar nature of the binding processes for the ATP and ADP analogues (see Discussion). In the next transition, $(H–N)_1$↔$(H–N)_2$, $\Delta H_2$ and $\Delta S_2$ are positive, suggesting that a process of a nature different from that of the first binding step is observed in the binding of both cofactors (see Discussion). On the other hand, changes in the thermodynamic functions in the third transition, $(H–N)_2 \leftrightarrow (H–N)_3$, differ for the association of TNP-ATP versus TNP-ADP (Table 3). Both $\Delta H_3$ and $\Delta S_3$ are positive for the ATP analogue, while $\Delta H_3 \approx 0$ for the ADP analogue. The absence of magnesium significantly affects the energetics of all reaction steps, although differently for ATP versus ADP analogues. The apparent enthalpy change, $\Delta H_1$, negative in the presence of $Mg^{2+}$, is now ~0, for TNP-ATP, while $\Delta H_1$ becomes even more negative in the case of TNP-ADP. The apparent enthalpy and entropy changes for the $(H–N)_1 \leftrightarrow (H–N)_2$ transition become very large and positive for both analogues. On the other hand, the values of $\Delta H_3$ and $\Delta S_3$ become negative, with a particular dramatic change occurring in the case of the ADP analogue (Table 3) (see Discussion).

## Global Conformations of the RepA Helicase Free and in the Presence of the ATP and ADP Analogues, in the Absence of Magnesium

To further address the dramatic effect of magnesium on the energetics and dynamics of binding of the nucleotide cofactor to the RepA helicase, we performed the analytical sedimentation velocity studies that provide direct information about the hydrodynamic properties of a macromolecule (21). In turn, the hydrodynamic properties reflect global conformational states of the macromolecule in solution. Sedimentation velocity profiles of the RepA helicase alone, in the absence of magnesium, are shown in Figure 5a. The total enzyme concentration is $1 \times 10^{-5}$ M (hexamer). To obtain the apparent average sedimentation coefficient, $s_{20,w}$, the sedimentation velocity scans have been analyzed using the time-derivative approach, which provides an $s_{20,w}$ of 7.8±0.1 S (21). Such a nonlinear least-squares fit, for RepA alone, is shown in Figure 5b. The obtained value of $s_{20,w}$ is significantly lower than the $s_{20,w}$ of 8.3 ± 0.1 S, determined for the enzyme in the presence of $Mg^{2+}$, and indicates a profoundly changed global structure of the enzyme (see Discussion) (21).

In the case of the RepA–TNP–cofactor complex, we can utilize the fact that the absorption spectrum of the cofactor has a maximum at 410 nm, which allows us to directly monitor the sedimentation of the nucleotide in the complex with the enzyme, without the interference of the protein absorbance (26). Sedimentation velocity profiles of the RepA–TNP-ADP complex in buffer T5 (pH 7.6 and 10 °C), in the absence of magnesium, are shown in Figure 5c. The total protein and cofactor concentrations are $1 \times 10^{-5}$ M (hexamer) and $6.5 \times 10^{-6}$ M, respectively. At the selected RepA and TNP-ADP concentrations, the cofactor completely saturates the protein and, on average, one cofactor molecule is associated with the enzyme. The apparent average sedimentation coefficient, $s_{20,w}$, of the RepA–TNP-ADP complex has been obtained using the time-derivative approach (Figure 5d), which provides an $s_{20,w}$ of 8.7 ± 0.1 S. Analogous studies with TNP-ATP, in the absence of $Mg^{2+}$, provided an $s_{20,w}$ of 8.4 ± 0.1 S (data not shown). It is evident that the presence of the nucleotides

strongly affects the global conformation of the RepA hexamer (21). Moreover, the effect is different for the ATP versus ADP analogue (see Discussion).

### Dynamics of Binding of the ATP and ADP Analogues to the Single, Noninteracting Nucleotide-Binding Site of the RepA Helicase in the Presence of the ssDNA

The RepA helicase acquires a significantly higher affinity for the ssDNA in the presence of ATP or ATP nonhydrolyzable analogues than in the absence of the cofactors (12,21,53). Moreover, binding of only a single NTP cofactor molecule to the hexamer is necessary to induce the high-ssDNA affinity state (21). Nevertheless, the binding of the ssDNA 20-mer to the enzyme, whose length corresponds to the site size of the enzyme–ssDNA complex, is characterized by the binding constant, $K_{20}$, in the range of $5\times 10^3$ to $1 \times 10^4$ $M^{-1}$, which allows us to address the effect of the ssDNA on the dynamics of binding of the nucleotide to the enzyme–ssDNA complex, by performing experiments in the presence of elevated concentrations of the nucleic acid (21). The stopped-flow measurements of the binding of the ATP and ADP analogues to the RepA helicase, in the presence of the ssDNA 20-mer, $dT(pT)_{19}$, have been examined as described above (35,38–49). The kinetic traces required a double-exponential function (eq 3) to adequately represent the experimental curves. Also, in the high-protein concentration range, a part of the fluorescence increase of the analogue occurs in the time range, which is beyond the time resolution of the stopped-flow measurement (data not shown).

The dependence of the reciprocal relaxation times, $1/\tau_2$ and $1/\tau_3$, as a function of the total RepA helicase concentration, $[RepA]_T$ (protomer), and in the presence of the ssDNA 20-mer, $dT(pT)_{19}$ [$7 \times 10^{-5}$M (oligomer)] (final concentration), for the association reaction of TNP-ATP with the enzyme, is shown in Figure 6a,b. The values of $1/\tau_2$ increase with $[RepA]_T$, showing only slightly marked hyperbolic behavior (35, 38–49). However, as discussed above, these data and the presence of the fast preceding process indicate that $1/\tau_2$ describes the intramolecular transition of the formed complex (35, 50, 51). The hyperbolic dependence of $1/\tau_3$ on $[RepA]_T$ clearly indicates an internal isomerization of the complex. The dependence of the normalized individual amplitudes, $A_1$, $A_2$, and $A_3$, on the logarithm of the total concentration of RepA helicase, is shown in Figure 6c (47–49). Amplitude $A_1$ of the fast, unresolved process appears only at high values of $[RepA]_T$ and significantly contributes to the total amplitude of the relaxation process in the high-protein concentration range. Amplitude $A_2$ dominates the observed total amplitude, $A_T$, at low enzyme concentrations. However, the values of $A_2$ sharply decrease with the increase in $[RepA]_T$ and become negative in the high-protein concentration range. Amplitude $A_3$ is positive and appears only at higher protein concentrations. Nevertheless, $A_3$ gradually increases with an increasing protein concentration. Such behavior of the reciprocal relaxation times and the individual amplitudes is in excellent agreement with the proposed kinetic mechanism (eq 5) (35, 50, 51). Analogous experiments have been performed for the association of the ADP analogue with the RepA helicase (data not shown). The obtained kinetic and spectroscopic parameters for binding of TNP-ATP and TNP-ADP to the single, noninteracting nucleotide-binding site of the RepA helicase are included in Table 1.

In the case of TNP-ATP, the value of the partial equilibrium constant ($K_1 \approx 6 \times 10^4$ $M^{-1}$) is approximately 1 order of magnitude higher than that observed in the absence of the ssDNA (Table 1). There is also a dramatic increase in the value of $K_2$, from ~118 to ~2650. Thus, both $K_1$ and $K_2$ strongly contribute to the overall increase in the affinity of the ATP analogue for the nucleotide-binding site (Table 1). The large increase in $K_2$ results from the decrease in $k_{-2}$, by a factor of ~25 in the presence of the nucleic acid, while the value of $k_2$ is slightly diminished under the same conditions (Table 1). On the other hand, the value of $K_3$ is only ~0.1; i.e., it is diminished by a factor of ~25, as compared to the value determined in the absence of the nucleic acid, and makes a negative contribution to the overall free

energy of binding (Table 1). Changes in the internal energetics and dynamics are accompanied by changes of the environment of the cofactor in the binding site. The relative fluorescence intensity of intermediate $(H–N)_1$ is significantly increased, while that of $(H–N)_2$ is only slightly affected by the presence of the ssDNA.

However, the fluorescence intensity of the third intermediate, $(H–N)_3$, is diminished by a factor of ~5, as compared to the intensity of the corresponding intermediate in the absence of the DNA. The effect of the ssDNA on the binding of TNP-ADP to the RepA helicase is very different. The $K_1$ value of $\approx 8\times 10^3 M^{-1}$ is lower than that observed in the absence of the ssDNA (Table 1). The presence of the nucleic acid does not affect $K_2$ and only slightly increases the value of $K_3$. As a result, the overall affinity of the ADP analogue for the nucleotide-binding site remains very similar to that observed in the absence of the ssDNA (Table 1). Although the relative fluorescence intensity of $(H–N)_1$ is significantly increased, the fluorescence intensities of $(H–N)_2$ and $(H–N)_3$ are only slightly affected by the presence of the nucleic acid (see Discussion).

## Fractional Distributions of Intermediates of the Nucleotide Cofactor Binding to the Single, Noninteracting Nucleotide-Binding Site of the RepA Helicase in the Presence of Magnesium

The distributions of the intermediates during the time course of the reaction in the binding of ATP and ADP analogues to the RepA hexamer, at 10 °C and in the presence of magnesium, are shown in panels a and b of Figure 7, respectively. The concentrations of the intermediates are normalized as molar fractions of the total concentration of the nucleotide cofactors. At the selected protein concentration, the nucleotide cofactors are saturated with the helicase. We cannot access the dynamics of the fast bimolecular step, but we can address the maximum fractional contribution of $(H–N)_1$ by modeling the process as close to the diffusion-controlled reaction, with the determined partial equilibrium constant, $K_1$. Ina manner independent of the assumed diffusion-controlled character, the first, fast-forming intermediate, $(H–N)_1$, detectably contributes to the total population of the ATP analogue states over a large time span of the reaction. However, it does not constitute any significant fraction of the total cofactor population at equilibrium. Unlike $(H–N)_1$, intermediate $(H–N)_2$ constitutes a significant (~27%) portion of the total population of the ATP analogue at the equilibrium state (Figure 7a). The third intermediate, $(H–N)_3$, dominates the population of the bound ATP cofactor at the equilibrium state (see Discussion). The fractional distributions of the ADP analogue intermediates (Figure 7b) are similar to the distributions of the ATP analogue. Higher temperature does not significantly affect the intermediate distributions of either cofactor (data not shown).

## Fractional Distributions of Intermediates of the Nucleotide Cofactor Binding to the Single, Noninteracting Nucleotide-Binding Site of the RepA Helicase in the Presence of the ssDNA

The fractional distributions of the intermediates during the time course of the reaction in the binding of ATP and ADP analogues to the RepA hexamer, in the presence of the ssDNA 20-mer, are shown in panels c and d of Figure 7, respectively. The contribution of $(H–N)_1$ to the total population of the ATP analogue is little affected by the presence of the ssDNA (Figure 7a,c). However, the contribution of $(H–N)_2$ is dramatically changed by the presence of the ssDNA and now constitutes ~91%of the total population in the equilibrium state (Figure 7c). Moreover, $(H–N)_3$, which dominates the population of the bound ATP cofactor at equilibrium, in the absence of the ssDNA (Figure 7a), is reduced to ~9% of the total population at equilibrium, in the presence of the nucleic acid (see Discussion). Unlike TNP-ATP, the presence of the ssDNA20-mer has a much less pronounced effect on the intermediate distributions of the RepA–ADP analogue complex (Figure 7d), as compared to the effect observed in the absence of the DNA (Figure 7b).

# DISCUSSION

## Multiple-Step Kinetic Mechanism of Binding of the Nucleotide Cofactor to the Single, Noninteracting Binding Site of the RepA Helicase

In the presence of magnesium, the kinetic mechanism of TNP-ATP and TNP-ADP binding to a single, noninteracting nucleotide-binding site on the RepA helicase is a minimum three-step, sequential process (eq 5). The sequential character of the mechanism indicates that transitions to different states of the protein occur as a response to the formation of the enzyme–nucleotide complex; i.e., conformational transitions of the RepA helicase are not present prior to the nucleotide binding but are induced by the cofactor (35,38–51). The observed mechanism is also similar to that of the analogous *E. coli* DnaB protein, which undergoes sequential conformational transitions in response to the nucleotide association, indicating that this is the general behavior of hexameric helicases; i.e., the global structure of the enzyme is under the strict control of the nucleotide cofactors (39,41). Nevertheless, the mechanism of binding of the nucleotide to the RepA helicase is simpler and the dynamcs of the transitions are faster than those observed in the case of the DnaB protein (41). Such mechanistic simplicity and much faster dynamics may reflect the limited number of functional engagements of the RepA protein, specifically geared for replication of the RSF1010 plasmid, as compared to the DnaB helicase, which is engaged in a multitude of functions, including different pathways in the replisome and primosome assemblies (6).

The largest increase in nucleotide fluorescence occurs in the formation of the $(H–N)_1$ intermediate, indicating a dramatic change in the environment around the cofactor in $(H–N)_1$, as compared to the bulk solution (25,54). Moreover, the first step is accompanied by a significant negative enthalpy change, indicating the presence of a conformational change(s) in the formed complex (Table 3). These results indicate that the observed first step cannot be a simple collision complex (41,55). The fact that the first step is beyond the time resolution of the stopped-flow technique indicates that the very binding process, including an additional conformational transition of the formed complex, is a very fast reaction occurring in a maximum of a few milliseconds.

The energetics and dynamics of the second step are different from the dynamics of the first step and strikingly different from those of the corresponding step in binding of the cofactor to the *E. coli* DnaB helicase (Table 1) (41). The partial equilibrium constant, $K_2$, is ~200 and ~120 for the ADP and ATP analogue, respectively. Thus, the second step contributes very substantially to the overall free energy of cofactor binding. The corresponding transition in the case of the DnaB helicase is characterized by a$K_2$ of ≈0.4–2.3, i.e., with very small, if any, favorable contribution to the overall affinity (41). Also, the rate constant $k_2$ is ~30 and 59 $s^{-1}$ for the ADP and ATP analogue, respectively, significantly larger than the values of ≈3–14 $s^{-1}$ observed for the nucleotide binding to the DnaB protein (Table 1) (41). The large value of $K_2$ results from the very low values of $k_{-2}$, which are more than 1 order of magnitude lower than that observed for the DnaB helicase (Table 1). Finally, the $(H–N)_2 \leftrightarrow (H–N)_3$ transition is also more energetically favorable and significantly faster than that determined for the DnaB helicase.

Recall that the RepA hexamer is characterized by an unusually strong stability, which distinguishes the enzyme from other hexameric helicases, including the DnaB helicase (10–14,53). A plausible explanation of the observed differences between these two analogous enzymes is that because the tight interactions between subunits of the RepA hexamer are already established prior to cofactor binding, the energetics and dynamics of the $(H–N)_1 \leftrightarrow (H–N)_2$ transition reflect the free energy of the cofactor binding and the specific cofactor-induced structural change. In the case of the DnaB hexamer, part of the free energy of binding and the $(H–N)_1 \leftrightarrow (H–N)_2$ transition are used to establish stronger intersubunit

interactions, leading to the observed, much lower favorable free energy change for cofactor binding, and also to the slower forward and faster backward rates of the transition, respectively. Notice, peculiar aspects of the observed kinetics of binding of the nucleotides to the RepA helicase are the close values of both $1/\tau_2$ and $1/\tau_3$, pointing to significant coupling of the two relaxation processes, which reflect isomerizations of the formed complex (Figure 3a,b). This is different from the DnaB helicase in which the relaxation times significantly differ (41). Such coupling would be expected for the system with very tight intersubunit interactions, which would increase the interdependence of the conformational changes induced by the nucleotide binding.

## The Bound Nucleotide Cofactors Experience Changes in the Structure of the Nucleotide-Binding Site, Which Depend on the Structure of the Phosphate Group

The fluorescence emission of the TNP group is very sensitive to the physical nature of the environment and is an excellent reporter of the polarity of the surroundings on Kosower's scale (54). For both the ATP and ADP analogues, the largest fluorescence increase in the cofactor occurs in the formation of $(H–N)_1$, indicating that the TNP group of the bound nucleotide is in the most hydrophobic environment in $(H–N)_1$ and both cofactors deeply enter the pocket of the binding site. Nevertheless, the $F_1$ value of ≈16 determined for TNP-ATP is significantly larger than the $F_1$ of ≈9 obtained for TNP-ADP, indicating that the ATP analogue is in a different state than the ADP analogue in $(H–N)_1$ (Table 1). The differences between the fluorescence intensities of the bound TNP-ATP and TNP-ADP are also present in the subsequent intermediates, $(H–N)_2$ and $(H–N)_3$. Thus, in spite of similar dynamics and energetics of intermediate formation, these data strongly suggest that the cofactor–enzyme complexes undergo a sequence of structural changes, which depends on the structure of the phosphate group of the cofactor. Similar differences between bound ATP and ADP analogues were previously observed for the DnaB helicase, reinforcing the notion of general mechanistic and structural responses of hexameric helicases to nucleotide binding (41).

## Different Apparent Enthalpy and Entropy Changes of the Binding Steps in the Nucleotide Cofactor Association with the RepA Helicase Indicate a Different Nature of the Formed Intermediates

The effect of temperature on binding of the nucleotide to the RepA helicase provides an additional strong indication of the different nature of the formed intermediates. In the presence of magnesium, the first reaction step is characterized by an apparent negative enthalpy and small entropy changes, for both ATP and ADP analogues (Table 3). Thus, the data show that the intrinsic nucleotide binding process of the RepA helicase, independent of the structure of the phosphate group, is apparently an enthalpy-driven process. The second step, $(H–N)_1 \leftrightarrow (H–N)_2$, is very different from the bimolecular association and is characterized by the apparent positive enthalpy and entropy changes (Table 3). As we discussed above, dramatically slower dynamics of the second step for both analogues, as compared to the bimolecular step, indicate that a global conformational change of the RepA helicase is dominating this transition (see above). The equally dramatic changes in the thermodynamic functions strongly support the conclusion that a process of a different nature, as compared to the bimolecular step, dominates the second step.

The data indicate that the accompanying conformational change of the RepA helicase in the $(H–N)_1 \leftrightarrow (H–N)_2$ transition is an entropy-driven process strongly opposed by the enthalpy changes. Such thermodynamic characteristics can be understood in the context of the unusually strong stability of the RepA hexamer, which requires perfectly matching protein–protein interfaces with multiple and energetically favorable interactions. Breaking such intersubunit engagements, as a result of a global conformational change, must be

energetically unfavorable. The large positive entropy change also suggests that the reorientation of subunits is accompanied by large changes in the hydration of the hexamer (21). This conclusion is supported by the fact that the $(H–N)_2$ intermediate is preferentially selected by the ssDNA bound to the enzyme, which requires opening of the hexameric structure (see below) (38,53).

The next step, $(H–N)_2 \leftrightarrow (H–N)_3$, is different for the ATP versus ADP analogue. For TNP-ATP, the transition is accompanied by apparent positive enthalpy and entropy changes. For the ADP analogue, the process is characterized by the apparent $\Delta H_3$ of ≈0 and positive $\Delta S_3$ (Table 3). Recall that the RepA helicase acquires the high ssDNA affinity only in the presence of ATP or ATP analogues (12,53). Thus, a possible explanation of this difference is that, in the case of the ATP analogue, a further conformational change in the enzyme occurs, which is energetically unfavorable and plays a role in the entry of DNA into the cross channel (see below).

## Binding of Magnesium Cations to the RepA Helicase Is Necessary for the Efficient Communication between Different Intermediates of the RepA Protein–Nucleotide Complex

The dramatic change in the sedimentation coefficient of the RepA hexamer, from ~8.3 S in the presence of magnesium to ~7.8 S in the absence of $Mg^{2+}$, indicates a very significant change in the global conformation of the RepA hexamer and provides direct evidence of the specific $Mg^{2+}$ binding to the protein (14). The large extent of the change strongly suggests a profound modification of the intersubunit interactions (21). Binding of a single nucleotide molecule to the RepA helicase, in the absence of magnesium, increases the sedimentation coefficient to ~8.3 and ~8.7 S for TNP-ATP and TNP-ADP, respectively. First, these data show that the global conformation of the RepA hexamer is dramatically affected by the nucleotide binding to one of the six nucleotide-binding sites of the protein (21). Second, the effect is dependent upon the structure of the phosphate group; i.e., the bound ATP analogue molecule induces a different conformational state than the ADP analogue (14,21). Third, these results indicate that the diminished nucleotide affinity, in the absence of $Mg^{2+}$, results from the fact that part of the binding free energy is used to induce conformational changes in the entire hexamer (see below).

The kinetic data provide information about the effect of $Mg^{2+}$ on the dynamics and internal energetics among particular intermediates of the protein–nucleotide complexes (14). The absence of $Mg^{2+}$ decouples the relaxation processes, which is the first indication of a weakened interdependence between conformational states of the enzyme induced by the cofactors (Figure 4). Magnesium cations are not necessary for the bimolecular step, which is even more energetically favorable in the absence of $Mg^{2+}$ (Table 2). However, $Mg^{2+}$ cations differently affect the energetics of the binding step for the ATP versus ADP analogue. The partial equilibrium constant, $K_1$, is by factors of ~20 and ~6 higher in the absence of magnesium, for TNP-ATP and TNP-ADP, respectively, as compared to the values of $K_1$ in the presence of $Mg^{2+}$ (Tables 1 and 2). Moreover, the absence of $Mg^{2+}$ differently affects the apparent enthalpy and entropy changes of the bimolecular step for the ATP versus ADP analogue (Table 3). Similarly, the effect of $Mg^{2+}$ on the third step, $(H–N)_2 \leftrightarrow (H–N)_3$, is different for TNP-ATP, as compared to that of TNP-ADP (Table 2). These results support the conclusion that the nature of the intermediates, $(H–N)_1$ and $(H–N)_3$, depends upon the structure of the phosphate group of the cofactor (see above).

However, the diminished overall affinity of the cofactors in the absence of $Mg^{2+}$ predominantly originates from the staggering diminishing of the values of $K_2$ by more than two 2 orders of magnitude, similar for both cofactors. Moreover, the rate constant, $k_2$, is diminished by approximately 1 order of magnitude. Such dramatic changes in the efficiency and dynamics of the $(H–N)_1 \leftrightarrow (H–N)_2$ transition indicate that the role of the $Mg^{2+}$ cations

bound to the enzyme is to induce and/or mediate efficient and fast contacts between the subunits of the enzyme, in spite of the fact that $Mg^{2+}$ is not necessary for the stability of the hexameric structure. In the context of the hydrodynamic data, the kinetic results indicate that global conformational change induced by cofactor binding predominantly occurs in the $(H–N)_1 \leftrightarrow (H–N)_2$ transition. Nevertheless, although the dynamics and energetics of the $(H–N)_1 \leftrightarrow (H–N)_2$ transition are independent of the structure of the phosphate group, the structure of $(H–N)_2$ is, as indicated by the very different fluorescence intensity of TNP-ATP and TNP-ADP in $(H–N)_2$ (see below).

## The Bound ssDNA Preferentially Selects a Single Intermediate from the RepA–ATP Analogue Complexes

Allosteric interactions between the nucleotide-binding site and the DNA-binding site of a helicase control the affinity of the enzyme for the nucleic acid and are a crucial part of the free energy transduction mechanisms of the enzyme (1–7,12,53). The RepA helicase acquires the high ssDNA affinity in the presence of ATP or ATP analogues, while ADP has only a modest effect, if any, on the association of the enzyme with the nucleic acid. In a thermodynamic equilibrium system, the opposite must also be true; i.e., the bound DNA will affect the dynamics and energetics of the ATP analogue association, while the effect of the nucleic acid on the binding of the ADP analogue to the enzyme should be much less pronounced.

In the case of TNP-ATP, the presence of the bound ssDNA 20-mer affects both the intermediate distribution during the time course of the reaction and the intermediate distribution in the equilibrium state (Figure 7a,c). The value of partial equilibrium constant $K_1$ is 1 order of magnitude larger in the presence of the ssDNA than in the absence of the nucleic acid (Table 1). Such a pronounced effect of the bound nucleic acid on the value of $K_1$ and a significant increase in the relative fluorescence intensity of the cofactor in $(H–N)_1$ indicate that the allosteric interactions between the nucleotide-binding site and the DNA-binding site are quickly established, within no more than a few milliseconds, in the initial stages of formation of the tertiary complex, RepA ATP analogue–ssDNA. However, the $H + N \leftrightarrow (H–N)_1$ step is still very fast; i.e., intermediate $(H–N)_1$ must be short-lived, strongly suggesting that allosteric interactions occur with the ssDNA bound in the outer DNA-binding site of the helicase (38, 56).

Nevertheless, the most dramatic effect is observed in the case of the partial equilibrium constant, $K_2$, which is increased by a factor of ~20 in the presence of the ssDNA (Table 1). The increase in $K_2$ results from the large decrease in the value of the backward rate constant, $k_{-2}$. Such a dynamic behavior would be expected for the transition, which is an intrinsic property of the enzyme–cofactor complex (see above), where the allosteric interactions between the nucleotide-binding site and the DNA-binding site additionally lock the cofactor in $(H–N)_2$, leading to the lower value of $k_{-2}$. Notice that the fluorescence intensity of $(H–N)_2$ is only slightly affected by the DNA, indicating that the DNA binds to the conformation induced by the cofactor.

On the other hand, the value of $K_3$ is diminished by a factor of ~25, as compared to the value determined in the absence of the DNA (Table 1). This occurs mainly through the large decrease in rate constant $k_3$ and a significantly increased value of $k_{-3}$. Moreover, the fluorescence intensity of the $(H–N)_3$ intermediate is diminished by a factor of ~5, as compared to the intensity of the corresponding intermediate in the absence of the DNA, indicating that the allosteric interactions affect the structure of the enzyme–cofactor complex. Thus, the presence of the nucleic acid slows the rate of the transition to the $(H–N)_3$ intermediate and dramatically decreases the efficiency of its formation. As a result, the contribution of $(H–N)_2$ constitutes ~91%of the total population of the bound ATP analogue

at the equilibrium state, while the analogous contribution of $(H–N)_3$ is profoundly reduced (Figure 7a,c). In other words, the bound nucleic acid preferentially selects $(H–N)_2$, i.e., the intermediate which results from a large conformational transition of the enzyme (see above), from all other intermediates of the RepA helicase–ATP analogue association reaction. Because the entry of the DNA into the cross channel is accompanied by a local opening of the hexameric structure of the RepA helicase, the $(H–N)_1 \leftrightarrow (H–N)_2$ transition, in the case of the ATP analogue, must constitute a prelude to the opening of the hexameric structure of the enzyme in the absence of the nucleic acid (38,53,56).

In the case of TNP-ADP, the value of $K_1$ is even slightly lower in the presence of the nucleic acid, as compared to the value observed in the absence of the ssDNA (Table 1). Nonetheless, the relative fluorescence intensity of $(H–N)_1$ is significantly increased in the presence of the DNA, indicating that the allosteric interactions between the nucleotide-binding site and the DNA-binding site do occur. Similarly, the nucleic acid does not affect $K_2$, slightly increases the value of $K_3$, and has little effect on the fluorescence intensities of $(H–N)_2$ and $(H–N)_3$ (Table 1). As a result, the fractional distributions of these intermediates during the time course of the reaction and in the equilibrium state are very similar to the fractional distributions determined in the absence of the DNA (Figure 7b,d). The obtained results indicate that, in the presence of the DNA, all transitions observed in the binding of nucleotides to the RepA helicase become sensitive to the structure of the phosphate group of the cofactor, with the initial testing of the structure of the phosphate group already occurring in the initial stage of the reaction in $(H–N)_1$, while the final major testing occurs in $(H–N)_2$.

A schematic model of the preferential selection of a single intermediate of the RepA helicase–NTP complex, which can account for the data obtained in this work, is depicted in Figure 8. The single NTP molecule binds to an independent nucleotide-binding site forming $(H–N)_1$ (13,14). The $(H–N)_1$ intermediate has an increased affinity for the nucleic acid, which is bound in the outer DNA-binding site of the enzyme. Nevertheless, $(H–N)_1$ is short-lived. The subsequent transition to $(H–N)_2$ is fast and energetically very favorable. The enzyme is locked in $(H–N)_2$ because of the slow rates back to $(H–N)_1$ and forward to $(H–N)_3$. In the equilibrium state, $(H–N)_2$ is preferentially selected by the single-stranded conformation of the enzyme-bound DNA. The selection process may include additional conformational transitions of the $(H–N)_2$–ssDNA complex, which, for the sake of simplicity, are not included in Figure 8 (56). A small fraction of the formed complex transforms into $(H–N)_3$. Nevertheless, the $(H–N)_2 \leftrightarrow (H–N)_3$ transition is slow and allows the efficient binding of the nucleic acid to $(H–N)_2$.

## Acknowledgments

We thank Gloria Drennan Bellard for her help in preparing the manuscript.

## References

1. Lohman TM, Bjornson KP. Mechanisms of Helicase-Catalyzed DNA Unwinding. Annu Rev Biochem. 1996; 65:169–214. [PubMed: 8811178]
2. Baker TA, Funnell BE, Kornberg A. Helicase action of dnaB protein during replication from the *Escherichia coli* chromosomal origin *in vitro*. J Biol Chem. 1987; 262:6877–6885. [PubMed: 3032979]
3. Enemark EJ, Joshua-Tor L. On Helicases and Other Motor Proteins. Curr Opin Struct Biol. 2008; 18:243–257. [PubMed: 18329872]
4. von Hippel PH, Delagoutte E. Helicase Mechanisms and the Coupling of Helicases Within Macromolecular Machines. Part I: Structures and Properties of Isolated Helicases. Q Rev Biophys. 2002; 35:431–478. [PubMed: 12621862]

5. von Hippel PH, Delagoutte E. Helicase Mechanisms and the Coupling of Helicases Within Macromolecular Machines. Part II: Integration of Helicases Into Cellular Processes. Q Rev Biophys. 2003; 36:1–69. [PubMed: 12643042]
6. Heller RC, Marians KJ. Non-Replicative Helicases at the Replication Fork. DNA Repair. 2007; 6:945–952. [PubMed: 17382604]
7. LeBowitz JH, McMacken R. The *Escherichia coli* dnaB Replication Protein Is a DNA Helicase. J Biol Chem. 1986; 261:4738–4748. [PubMed: 3007474]
8. Guerry P, van Embden J, Falkow S. Molecular Nature of Two Nonconjugative Plasmids Carrying Drug Resistance Genes. J Bacteriol. 1974; 117:987–997. [PubMed: 4591964]
9. De Gaaf J, Crossa JH, Heffron F, Falkow S. Replication of the Nonconjugative Plasmid RSF1010 in *Escherichia coli* K-12. J Bacteriol. 1978; 134:1117–1122. [PubMed: 350840]
10. Scherzinger E, Ziegelin G, Barcena M, Carazo JM, Lurz R, Lanka E. The RepA Protein of Plasmid RSF1010 Is a Replicative DNA Helicase. J Biol Chem. 1997; 272:30228–30236. [PubMed: 9374507]
11. Niedenzu T, Roleke D, Bains Scherzinger E, Saenger W. Crystal Structure of the Hexameric Helicase RepA of Plasmid RSF1010. J Mol Biol. 2001; 306:479–487. [PubMed: 11178907]
12. Jezewska MJ, Galletto R, Bujalowski W. Interactions of the RepA helicase hexamer of plasmid RSF1010 with the ssDNA. Quantitative Analysis of Stoichiometries, Intrinsic Affinities, Cooperativities, and Heterogeneity of the Total ssDNA-Binding Site. J Mol Biol. 2004; 343:115–136. [PubMed: 15381424]
13. Jezewska MJ, Lucius AL, Bujalowski W. Binding of Six Nucleotide Cofactors to the Hexameric Helicase RepA Protein of Plasmid RSF1010. I. Direct Evidence of Cooperative Interactions Between the Nucleotide-Binding Sites of a Hexameric Helicase. Biochemistry. 2005; 44:3865–3876. [PubMed: 15751962]
14. Jezewska MJ, Lucius AL, Bujalowski W. Binding of Six Nucleotide Cofactors to the Hexameric Helicase RepA Protein of Plasmid RSF1010. II. Base Specificity, Nucleotide Structure, Magnesium, and Salt Effect on the Cooperative Binding of the Cofactors. Biochemistry. 2005; 44:3877–3890. [PubMed: 15751963]
15. Bujalowski W, Klonowska MM, Jezewska MJ. Oligomeric Structure of *Escherichia coli* Primary Replicative Helicase DnaB Protein. J Biol Chem. 1994; 269:31350–31358. [PubMed: 7989299]
16. Jezewska MJ, Kim US, Bujalowski W. Binding of *Escherichia coli* Primary Replicative Helicase DnaB Protein to Single-Stranded DNA. Long-Range Allosteric Conformational Changes within the Protein Hexamer. Biochemistry. 1996; 35:2129–2145. [PubMed: 8652555]
17. Dong F, Gogol EP, von Hippel PH. The Phage T4-coded DNA Replication Helicase (gp41) Forms a Hexamer Upon Activation By Nucleoside Triphosphate. J Biol Chem. 1995; 270:7462–7473. [PubMed: 7706292]
18. Gogol EP, Seifried SE, von Hippel PH. Structure and Assembly of the *Escherichia coli* Transcription Termination Factor Rho and Its Interactions With RNA. I. Cryoelectron Microscopy Studies. J Mol Biol. 1991; 221:1127–1138. [PubMed: 1719215]
19. Trakselis MA, McGeoch AT, Laskey RA, Bell SD. Organization of an Archaeal MCM Complex on DNA and Implications For Helicase Mechanisms. Nat Struct Mol Biol. 2005; 12:756–762. [PubMed: 16116441]
20. Egelman EH, Yu X, Wild R, Hingorani MM, Patel SS. Bacteriophage T7 Helicase/Primase Proteins Form Rings Around Single-Stranded DNA that Suggest a General Structure for Hexameric Helicases. Proc Natl Acad Sci USA. 1995; 92:3869–3873. [PubMed: 7731998]
21. Marcinowicz A, Jezewska MJ, Bujalowski W. Multiple Global Conformational States of the Hexameric RepA Helicase of Plasmid RSF1010 With Different ssDNA-Binding Capabilities Are Induced by Different Numbers of Bound Nucleotides. Analytical Ultracentrifugation and Dynamic Light Scattering Studies. J Mol Biol. 2008; 375:386–408. [PubMed: 18022636]
22. Edelhoch H. Spectroscopic Determination of Tryptophan and Tyrosine in Proteins. Biochemistry. 1967; 6:1948–1954. [PubMed: 6049437]
23. Gill SC, von Hippel PH. Calculation of Protein Extinction Coefficients from Amino Acid Sequence Data. Anal Biochem. 1989; 182:319–326. [PubMed: 2610349]

24. Bujalowski W, Klonowska MM. Negative Cooperativity in the Binding of Nucleotides to *E. coli* Replicative Helicase DnaB Protein. Interactions with Fluorescent Nucleotide Analogs. Biochemistry. 1993; 32:5888–5900. [PubMed: 8504109]
25. Bujalowski W, Klonowska MM. Structural Characteristics of the Nucleotide Binding Site of *E. coli* Primary Replicative Helicase DnaB Protein. Studies with Ribose and Base-Modified Fluorescent Nucleotide Analogs. Biochemistry. 1994; 33:4682–4694. [PubMed: 8161526]
26. Lucius AL, Jezewska MJ, Bujalowski W. The *Escherichia coli* PriA Helicase Has Two Nucleotide-Binding Sites Differing in Their Affinities for Nucleotide Cofactors. 1. Intrinsic Affinities, Cooperativities, and Base Specificity of Nucleotide Cofactor Binding. Biochemistry. 2006; 45:7202–7216. [PubMed: 16752911]
27. Lucius AL, Jezewska MJ, Roychowdhury A, Bujalowski W. Kinetic Mechanisms of the Nucleotide Cofactor Binding to the Strong and Weak Nucleotide-Binding Site of the *Escherichia coli* PriA Helicase. 2. Biochemistry. 2006; 45:7217–7236. [PubMed: 16752912]
28. Lucius AL, Jezewska MJ, Bujalowski W. Allosteric Interactions Between the Nucleotide-Binding Sites and the ssDNA-Binding Site in the PriA Helicase–ssDNA Complex. 3. Biochemistry. 2006; 45:7237–7255. [PubMed: 16752913]
29. Galletto R, Rajendran S, Bujalowski W. Interactions of Nucleotide Cofactors with the *Escherichia coli* Replication Factor DnaC Protein. Biochemistry. 2000; 39:12959–12969. [PubMed: 11041861]
30. Huang SG, Weisshart K, Fanning E. Characterization of the Nucleotide Binding Properties of SV40 T Antigen Using Fluorescent 3′(2′)-O-(2,4,6-Trinitrophenyl)adenine Nucleotide Analogs. Biochemistry. 1998; 37:15336–15344. [PubMed: 9799494]
31. Jezewska MJ, Bujalowski W. A General Method of Analysis of Ligand Binding to Competing Macromolecules Using the Spectroscopic Signal Originating from a Reference Macromolecule. Application to *Escherichia coli* Replicative Helicase DnaB Protein-Nucleic Acid Interactions. Biochemistry. 1996; 35:2117–2128. [PubMed: 8652554]
32. Jezewska MJ, Rajendran S, Bujalowski W. Strand Specificity in the Interactions of *Escherichia coli* Primary Replicative Helicase DnaB Protein with Replication Fork. Biochemistry. 1997; 36:10320–10326. [PubMed: 9254631]
33. Jezewska MJ, Rajendran S, Bujalowski W. Functional and Structural Heterogeneity of the DNA Binding of the *E. coli* Primary Replicative Helicase DnaB Protein. J Biol Chem. 1998; 273:9058–9069. [PubMed: 9535894]
34. Bujalowski, W.; Jezewska, MJ. Quantitative Determination of Equilibrium Binding Isotherms for the Multiple Ligand-Macromolecule Interactions Using Spectroscopic Methods. In: Gore, MG., editor. Spectrophotometry and Spectrofluorimetry: A Practical Approach. Vol. Chapter 5. Oxford University Press; New York: 2000. p. 141-165.
35. Bujalowski W. Thermodynamic and Kinetic Methods of Analyses of Protein–Nucleic Acid Interactions. From Simpler to More Complex Systems. Chem Rev. 2006; 106:556–606. [PubMed: 16464018]
36. Lakowicz, JR. Principles of Fluorescence Spectroscopy. 2. Kluwer Academic; New York: 1999. p. 185-233.
37. Azumi T, McGlynn SP. Polarisation of the Luminescence of Phenantrene. J Chem Phys. 1962; 37:2413–2420.
38. Bujalowski W, Jezewska MJ. Kinetic Mechanism of the Single-Stranded DNA Recognition by *Escherichia coli* Replicative Helicase DnaB Protein. Application of the Matrix Projection Operator Technique to Analyze Stopped-Flow Kinetics. J Mol Biol. 2000; 295:831–852. [PubMed: 10656794]
39. Rajendran S, Jezewska MJ, Bujalowski W. Multiple-step Kinetic Mechanism of DNA-independent ATP Binding and Hydrolysis by *Escherichia coli* Replicative Helicase DnaB Protein: Quantitative Analysis Using the Rapid Quench-flow Method. J Mol Biol. 2000; 303:773–795. [PubMed: 11061975]
40. Galletto R, Jezewska MJ, Bujalowski W. Multi-Step Sequential Mechanism of *E. coli* Helicase PriA Protein–ssDNA Interactions. Kinetics and Energetics of the Active ssDNA-Searching Site of the Enzyme. Biochemistry. 2004; 43:11002–11016. [PubMed: 15323559]

41. Bujalowski W, Jezewska MJ. Kinetic Mechanism of Nucleotide Cofactor Binding to *Escherichia coli* Replicative Helicase DnaB Protein. Stopped-Flow Kinetic Studies Using Fluorescent, Ribose-, and Base-Modified Nucleotide Analog. Biochemistry. 2000; 39:2106–2122. [PubMed: 10684661]
42. Galletto R, Bujalowski W. The *E. coli* Replication Factor DnaC Protein Exists in Two Conformations with Different Nucleotide Binding Capabilities. I. Determination of the Binding Mechanism Using ATP and ADP Fluorescent Analogues. Biochemistry. 2002; 41:8907–8920. [PubMed: 12102633]
43. Galletto R, Bujalowski W. Kinetics of the *E. coli* Replication Factor DnaC Protein–Nucleotide Interactions. II. Fluorescence Anisotropy and Transient, Dynamic Quenching Stopped-Flow Studies of the Reaction Intermediates. Biochemistry. 2002; 41:8921–8934. [PubMed: 12102634]
44. Bujalowski W, Jezewska MJ, Galletto R. Dynamics of Gapped DNA Recognition by Human Polymerase $\beta$. J Biol Chem. 2002; 277:20316–20327. [PubMed: 11912205]
45. Bujalowski W, Jezewska MJ. Kinetic Mechanism of Nucleotide Cofactor Binding to *Escherichia coli* Replicative Helicase DnaB Protein. Stopped-Flow Kinetic Studies Using Fluorescent, Ribose-, and Base-Modified Nucleotide Analog. Biochemistry. 2000; 39:2106–2122. [PubMed: 10684661]
46. Galletto R, Jezewska MJ, Bujalowski W. Kinetics of Allosteric Conformational Transition of a Macromolecule Prior to Ligand Binding. Analysis of Stopped-Flow Kinetic Experiments. Cell Biochem Biophys. 2005; 42:121–144. [PubMed: 15858229]
47. Bujalowski W, Jezewska MJ, Galletto R. Dynamics of Gapped DNA Recognition by Human Polymerase $\beta$. J Biol Chem. 2002; 277:20316–20327. [PubMed: 11912205]
48. Jezewska MJ, Galletto R, Bujalowski W. Rat Polymerase $\beta$ Gapped DNA Interactions: Antagonistic Effects of the 5′ Terminal $PO_4^-$ Group and Magnesium on the Enzyme Binding to the Gapped DNAs with Different ssDNA Gaps. Cell Biochem Biophys. 2003; 38:125–160. [PubMed: 12777712]
49. Galletto R, Jezewska MJ, Bujalowski W. Kinetic Mechanism of Rat Polymerase $\beta$–dsDNA Interactions. Fluorescence Stopped-Flow Analysis of the Cooperative Ligand Binding to a Two-Site One-Dimensional Lattice. Biochemistry. 2005; 44:1251–1267. [PubMed: 15667219]
50. Bernasconi, CJ. Relaxation Kinetics. Academic Press; New York: 1976. p. 98-129.
51. Hammes, GG.; Schimmel, PR. The Enzymes Kinetics and Mechanism. Vol. II. Academic Press; New York: 1970. p. 67-114.
52. Connors, KA. The Study of Reaction Rates in Solution. VCH Publishers; New York: 1990. Chemical Kinetics; p. 133-186.
53. Marcinowicz A, Jezewska MJ, Bujalowski PJ, Bujalowski W. The Structure of the Tertiary Complex of the RepA Hexameric Helicase of Plasmid RSF1010 with the ssDNA and Nucleotide Cofactors in Solution. Biochemistry. 2007; 46:13279–13296. [PubMed: 17939681]
54. Kosower EM. The Effect of Solvent on Spectra. II. Correlation of Spectral Absorption Data with Z-Values. J Am Chem Soc. 1958; 80:3253–3260.
55. Moore, JW.; Pearson, RG. Kinetics and Mechanism. John Wiley & Sons; New York: 1981. p. 192-234.
56. Andreeva IE, Szymanski MR, Jezewska MJ, Galletto R, Bujalowski W. Dynamics of the ssDNA Recognition by the RepA Hexameric Helicase of Plasmid RSF1010. Analyses Using Fluorescence Stopped-Flow Intensity and Anisotropy Methods. J Mol Biol. 2009; 388:751–775. [PubMed: 19289128]

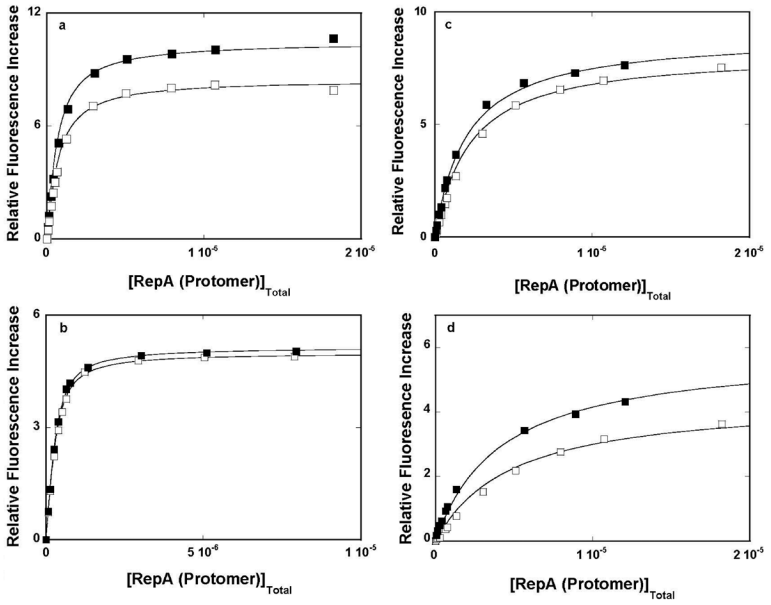


**Figure 1.**

(a) Fluorescence titrations ($\lambda_{ex}$ = 410 nm, and $\lambda_{ex}$ = 560 nm) of TNP-ATP with the RepA helicase in buffer T5, containing 5 mM $MgCl_2$, at 10 (□) and 20 °C (■). (b) Fluorescence titrations of TNP-ADP with the RepA helicase in buffer T5, containing 5mM $MgC1_2$, at 10 (□) and 20 °C (■). (c) Fluorescence titrations of TNP-ATP with the RepA helicase in buffer T5, in the absence of magnesium, at 10 (□) and 20°C (■). (d) Fluorescence titrations of TNP-ADP with the RepA helicase in buffer T5, in the absence of magnesium, at 10 (□) and 20°C(■). The solid lines in all panels are the nonlinear least-squares fits of the experimental titration curves to a single-site isotherm (eq 4) with the binding constant $K_{ov}$ and the maximum relative fluorescence change, $\Delta F_{max}$, as fitting parameters. The concentrations of the nucleotide cofactors are $3 \times 10^{-7}$ M. The concentration of the RepA hexamer is expressed as protein protomers. The obtained binding constants and spectroscopic parameters are included in Tables 1 and 2.

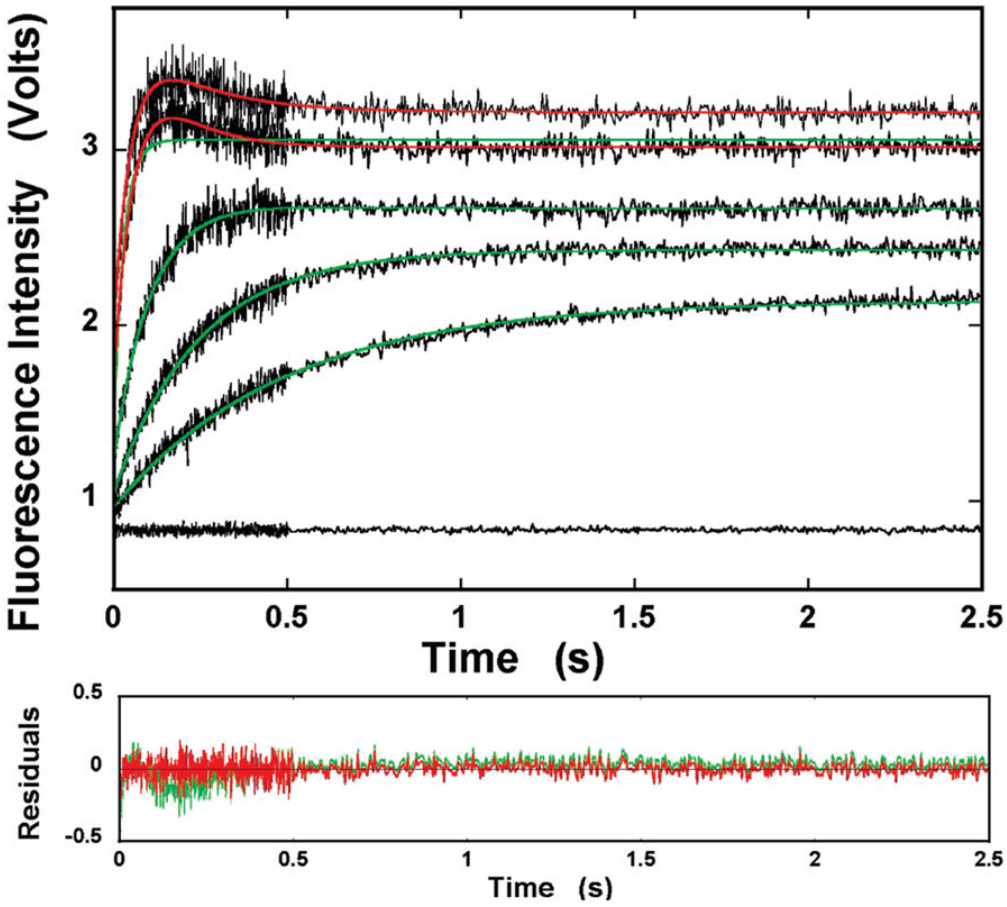


**Figure 2.**

Fluorescence stopped-flow kinetic traces (top), recorded in two time bases, 0.5 and 2.0 s, after the RepA helicase had been mixed with TNP-ATP in buffer T5, containing 5 mM $MgCl_2$ ($\lambda_{ex}$= 408 nm, and $\lambda_{em}$ > 500 nm). The final concentrations of the RepA helicase (protomer) are, from the top, $12\times 10^{-5}$, $9 \times 10^{-5}$, $3 \times 10^{-5}$, $1.2 \times 10^{-5}$, and $0.6 \times 10^{-5}$ M. The final concentration of the nucleotide is $5 \times 10^{-7}$ M. The solid green and red lines are the single-exponential and double-exponential, nonlinear least-squares fits, respectively, of the experimental curves, using eq 3. The bottom panel shows the deviations of the experimental curve from the fit using the single-exponential (green) and double-exponential functions (red) for the sample containing $9 \times 10^{-5}$ M (protomer) RepA helicase.

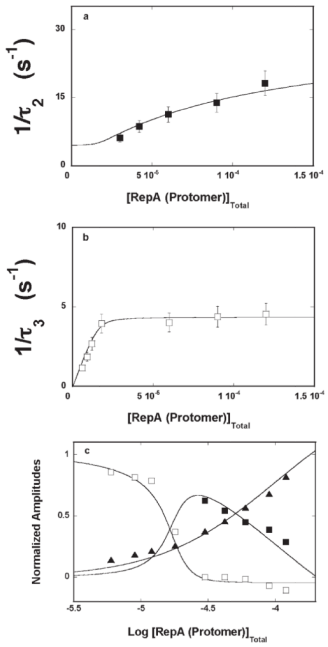


**Figure 3.**

Dependence of the reciprocal relaxation times for the binding of TNP-ATP to the RepA heliease in buffer T5 (10 °C), containing 5 mM $MgCl_2$, on the total concentration of the enzyme (protomer): (a) $1/\tau_2$ (■) and (b) $1/\tau_3$ (□). (c) Dependence of the individual normalized relaxation amplitudes $A_1$ (▲), $A_2$ (■), and $A_3$ (□), of the kinetic process of binding of TNP-ATP to the RepA helicase in buffer T5 (10 °C), containing 5 mM $MgCl_2$, on the logarithm of the total concentration of the enzyme (protomer). The solid lines in panels a, b, and c are nonlinear least-squares fits of the experimental data to the three-step sequential mechanism, defined by eq 5. The obtained kinetic and spectroscopic parameters are included in Table 1 (details in the text). The error bars are standard deviations obtained from three or four independent experiments.

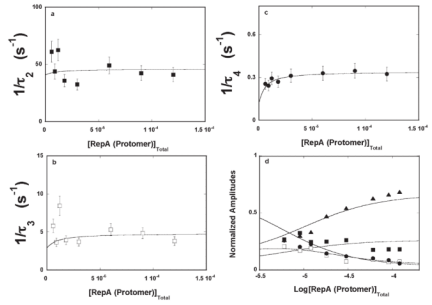


**Figure 4.**

Dependence of the reciprocal relaxation times for the binding of TNP-ATP to the RepA helicase in buffer T5 (10 °C), in the absence of magnesium, on the total concentration of the enzyme (protomer): (a) $1/\tau_2$ (■), (b) $1/\tau_3$ (□), and (c) $1/\tau_4$ (●). (d) Dependence of the individual normalized relaxation amplitudes $A_1$ (▲), $A_2$ (■), $A_3$ (□), and $A_4$ (●) of the kinetic process of binding of TNP-ATP to the RepA helicase in buffer T5 (10 °C), in the absence of magnesium, on the logarithm of the total concentration of the enzyme (protomer). The solid lines in panels a–d are nonlinear least-squares fits of the experimental data to the four-step sequential mechanism, defined by eq 9. The obtained kinetic and spectroscopic parameters are included in Table 2 (details in the text). The error bars are standard deviations obtained from three or four independent experiments.

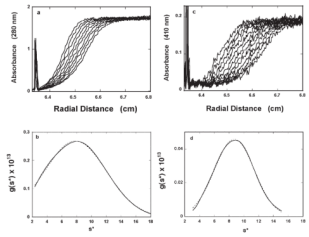


**Figure 5.**

(a) Absorption profiles, recorded at 280 nm, of analytical sedimentation velocity runs of the RepA belicase alone, in buffer T5 (pH 7.6 and 10 °C), in the absence of magnesium. The total protein concentration is $1 \times 10^{-5}$ M (hexamer). (b) The solid line is the apparent average sedimentation coefficient distribution $g(s^*)$, as a function of the radial sedimentation coefficient coordinate, $s^*$, obtained from time derivatives of the RepA sedimentation profiles recorded at 280 nm, in buffer T5 (pH 7.6 and 10 °C), in the absence of magnesium (35000 rpm). The dashed line is the nonlinear least-squares fit of the experimental distribution using the time-derivative method. Both plots are corrected for the solution conditions (details in the text). (c) Absorption profiles, recorded at 410 nm, of analytical sedimentation velocity runs of the RepA helicase–TNP-ADP complex, in buffer T5 (pH 7.6 and 10 °C), in the absence of magnesium. The total protein and cofactor concentrations are $1 \times 10^{-5}$ M (hexamer) and $6.5 \times 10^{-6}$ M, respectively. (d) The solid line is the apparent average sedimentation coefficient distribution, $g(s^*)$, as a function of the radial sedimentation coefficient coordinate, $s$, obtained from time derivatives of sedimentation profiles of the RepA–TNP-ADP complex recorded at 410 nm, in buffer T5 (pH 7.6 and 10 °C), in the absence of magnesium (35000 rpm). The dashed line is the nonlinear least-squares fit of the experimental distribution using the time-derivative method. Both plots are corrected for the solution conditions (details in the text).

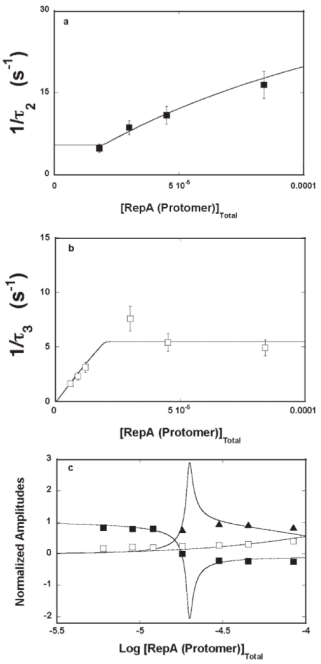


**Figure 6.**

Dependence of the reciprocal relaxation times for the binding of TNP-ATP to the RepA helicase in buffer T5 (10 °C), containing 5mM $MgCl_2$ and $7 \times 10^{-5}$M(oligomer) ssDNA 20-mer, $dT(pT)_{19}$, on the total concentration of the enzyme (protomer): (a) $1/\tau_2$ (■) and (b) $1/\tau_3$ (□). (c) Dependence of the individual normalized relaxation amplitudes, $A_1$ (▲), $A_2$ (■), and $A_3$ (□), of the kinetic process of binding of TNP-ADP to the RepA helicase in buffer T5 (10 °C), containing 5mM $MgC1_2$ and $7\times 10^{-5}$M(oligomer) ssDNA 20-mer, $dT(pT)_{19}$, on the logarithm of the total concentration of the enzyme (protomer). The solid lines in panels a–c are nonlinear least-squares fits of the experimental data to the three-step sequential mechanism, defined by eq 5. The obtained kinetic and spectroscopic parameters are included in Table 1 (details in the text). The error bars are standard deviations obtained from three or four independent experiments.

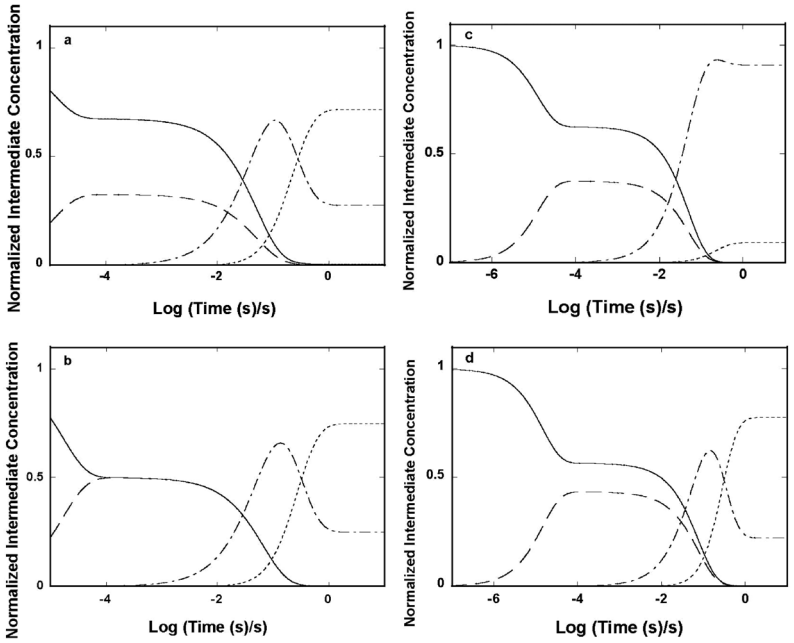


**Figure 7.**

(a) Computer simulation of the time course of the fractional concentration distribution of different TNP-ATP intermediates, in the binding to the RepA hexamer helicase, using the determined rate constants included in Table 1, in buffer T5, containing 5mM $MgCl_2$, at 10 °C. (b) Analogous plots of the fractional concentration distributions of different TNP-ADP intermediates, in the binding to the RepA helicase, using the determined rate constants included in Table 1, at 10 °C. (c) Computer simulation of the time course of the fractional concentration distribution of different TNP-ATP intermediates, in the binding to the RepA hexamer helicase, using the determined rate constants included in Table 1, in buffer T5 (10 °C), containing 5 mM $MgCl_2$ and $7 \times 10^{-5}$ M (oligomer) ssDNA 20-mer, $dT(pT)_{19}$. (d) Computer simulation of the time course of the fractional concentration distribution of different TNP-ADP intermediates, in the binding to the RepA helicase, using the determined rate constants included in Table 1, in buffer T5 (10 °C), containing 5 mM $MgCl_2$ and $7 \times l0^{-5}$ M (oligomer) ssDNA 20-mer, $dT(pT)_{19}$. The selected total nucleotide cofactor concentration is $1 \times 10^{-7}$ M. The selected RepA helicase concentration is $1 \times 10^{-4}$ (protomer): free nucleotide cofactor (__), $(H–N)_1$ (__ __), $(H–N)_2$ (–––), and $(H–N)_3$ (---). The bimolecular step is modeled close to the diffusion-controlled reaction with a $k_1$ of $1 \times 10^8 M^{-1}$ and the $k_{-1}$ adjusted to give the experimentally obtained partial equilibrium constant, $K_1=k_1/k_{-1}$ (details in the text).

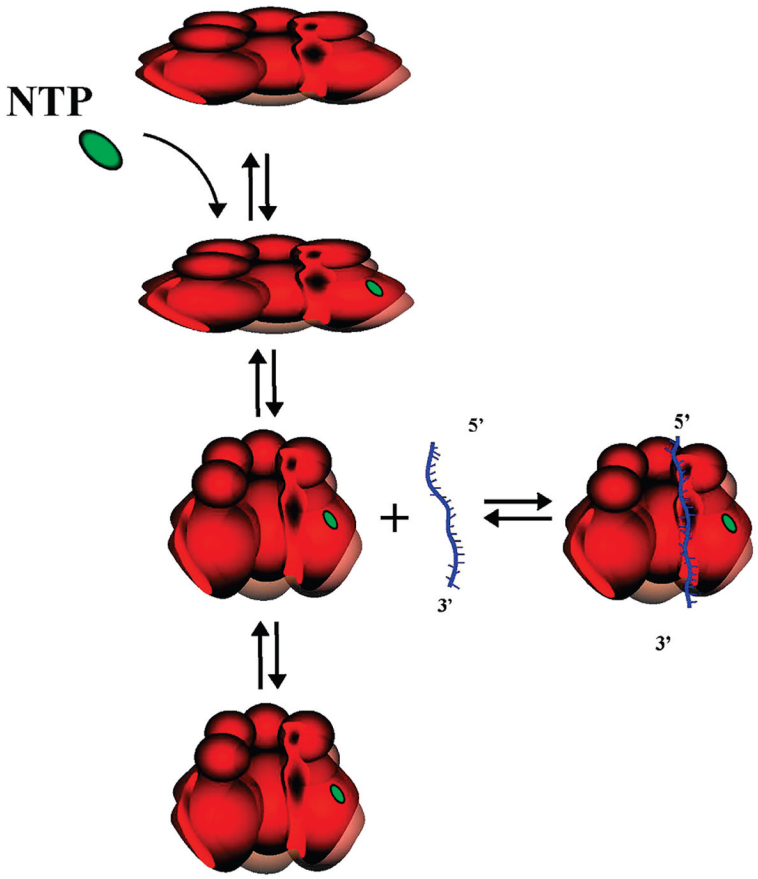


**Figure 8.**

Schematic model of the sequential kinetic mechanism of the NTP binding to the single, noninteracting nucleotide-binding site of the RepA hexamer and the selection of the intermediates of the reaction by the ssDNA, based on the data obtained in this work. Initially, all six nucleotide-binding sites are independent and equivalent (13,14). The single NTP molecule binds to an independent nucleotide-binding site forming the $(H–N)_1$ intermediate (13,14). The $(H–N)_1$ intermediate has a modestly increased affinity for the nucleic acid bound in the outer DNA-binding site of the enzyme (56). Nevertheless, $(H–N)_1$ is short-lived. The subsequent transition to the $(H–N)_2$ intermediate is fast and energetically very favorable. The $(H–N)_2$ intermediate is preferentially selected by the single-stranded conformation of the DNA and dominates the fractional distribution of the RepA–cofactor–ssDNA ternary complex in the equilibrium state. Only a small fraction of the formed complex transforms into the $(H–N)_3$ intermediate (details in the text).

**Table 1**

Thermodynamic, Kinetic, and Spectroscopic Parameters for the Binding of TNP-ADP and TNP-ATP to the RepA Hexameric Helicase of Plasmid RSF1010 in Buffer T5 (pH 7.6), Containing 5 mM $MgCl_2$, at Different Temperatures, and in the Presence of $7 \times 10^{-5}$ M (oligomer) ssDNA 20-mer, $dT(pT)_{19}$ (details in the text)[a]

| cofactor | $K_1$ ($M^{-1}$) | $K_2$ | $K_3$ | $k_2$ ($s^{-1}$) | $k_{-2}$ ($s^{-1}$) | $k_3$ ($s^{-1}$) | $k_{-3}$ ($s^{-1}$) | $K_{ov}$[b] ($M^{-1}$) | $F_1$ | $F_2$ | $F_3$ | $F_{max}$[b] |
|---|---|---|---|---|---|---|---|---|---|---|---|---|
| | | | | | TNP-ATP | | | | | | | |
| 10 °C | $(4.8\pm1.6) \times 10^3$ | 118 ±39 | 2.6± 0.8 | 59±12 | 0.5±0.1 | 3.9±0.8 | 1.5±0.3 | $(2.1 \pm0.4) \times 10^6$ | 15.8 ±0.3 | 13.9± 0.3 | 10.7±0.3 | 10.6±0.3 |
| 20 °C | $(3.3\pm1.1) \times 10^3$ | 138 ±46 | 3.4± 1.1 | 275±55 | 2.0±0.4 | 15.5±3.1 | 4.5±0.9 | $(2.0\pm0.4) \times 10^6$ | 14.6 ±0.3 | 10.8± 0.3 | 9.2±0.3 | 8.6±0.3 |
| 10 °C with $dT(pT)_{19}$ | $(6.0\pm 2) \times 10^4$ | 2650±850 | 0.1±0.03 | 53±10 | 0.02 ±0.003 | 0.5 ±1.3 | 5.0± 0.08 | $(1.8\pm 0.3) \times 10^7$ | 18.4 ±0.3 | 13.8± 0.3 | 2.3±0.3 | 11.8±0.3 |
| | | | | | TNP-ADP | | | | | | | |
| 10 °C | $(1.0\pm0.3) \times 10^4$ | 200 ±70 | 3.0± 1.0 | 30±6 | 0.15±0.03 | 3.3±0.6 | 1.1±0.2 | $(8.0 \pm1.6) \times 10^6$ | 8.9 ±0.3 | 6.3± 0.3 | 6.0±0.3 | 5.1±0.3 |
| 20 °C | $(7.5\pm2.5) \times 10^3$ | 267 ±87 | 3.0± 1.0 | 80±16 | 0.3±0.06 | 16±3 | 5.3±1.1 | $(8.0 \pm1.6) \times 10^6$ | 9.8 ±0.3 | 6.2± 0.3 | 5.9±0.3 | 5.0±0.3 |
| 10 °C with $dT(pT)_{19}$ | $(7.7\pm 2.6) \times 10^3$ | 200 ±70 | 3.5± 1.0 | 30±6 | 0.15±0.03 | 3.5±0.7 | 1±0.15 | $(6.9 \pm1) \times 10^6$ | 11.4±0.3 | 7.2±0.3 | 6.3±0.3 | 5.5 ±0.3 |

[a] Errors are standard deviations determined using three or four independent experiments.

[b] Determined in equilibrium fluorescence titrations.

**Table 2**

Thermodynamic, Kinetic, and Spectroscopic Parameters for the Binding of TNP-ADP and TNP-ATP to the RepA Hexameric Helicase of Plasmid RSF1010 in Buffer T5 (pH 7.6), in the Absence of Magnesium, at Different Temperatures (details in the text)[a]

| cofactor | $K_1$($M^{-1}$) | $K_2$ | $K_3$ | $K_4$ | $k_2$ ($s^{-1}$) | $k_{-2}$ ($s^{-1}$) | $k_3$ ($s^{-1}$) | $k_{-3}$ ($s^{-1}$) | $k_4$ ($s^{-1}$) | $k_{-4}$ ($s^{-1}$) | $K_{ov}$[b] ($M^{-1}$) | $F_1$ | $F_2$ | $F_3$ | $F_4$ | $F_{max}$[b] |
|---|---|---|---|---|---|---|---|---|---|---|---|---|---|---|---|---|
| | | | | | | | | TNP-ATP | | | | | | | | |
| 10°C | (1.0±0.3) ×$10^5$ | 0.25±0.08 | 3.4±1.1 | 3.5±1.2 | 7±1.4 | 28±5 | 12±2.4 | 3.5±0.7 | 0.53±0.1 | 0.15±0.03 | (5.0±1.1) ×$10^5$ | 7.0±0.3 | 7.0±0.3 | 22.8±0.3 | 10.2±0.3 | 9.0±0.3 |
| 20°C | (1.0±0.3)×$10^5$ | 1±0.3 | 3.0±1.0 | – | 30±6 | 30±6 | 2.1±0.4 | 0.7±0.14 | – | – | (5.0±1.1)×$10^5$ | 6.7±0.3 | 9.9±0.3 | 9.8±0.3 | – | 8.2±0.3 |
| | | | | | | | | TNP-ADP | | | | | | | | |
| 10°C | (6.1±2.0)×$10^4$ | 0.14±0.05 | 20±6 | – | 1±0.2 | 7±1.4 | 1±0.2 | 0.05±0.01 | – | – | (2.4±1.0)×$10^5$ | 7.7±0.3 | 11.6±0.3 | 6.6±0.3 | – | 6±0.3 |
| 20°C | (3.8±1.2)×$10^4$ | 1.7±0.5 | 2.0±0.7 | – | 3±0.6 | 1.8±0.4 | 0.30±0.06 | 0.15±0.03 | – | – | (2.3±0.5)×$10^5$ | 5.4±0.3 | 4.8±0.3 | 5.7±0.3 | – | 4.4±0.3 |

[a] Errors are standard deviations determined using three or four independent experiments.

[b] Determined in equilibrium fluorescence titrations.

**Table 3**

van't Hoff Enthalpies and Entropies Characterizing the Formation of Intermediates in the Binding of the Nucleotide Cofactors TNP-ADP and TNP-ATP to the RepA Helicase of Plasmid RSF1010 in Buffer T5 (pH 7.6), in the Presence or Absence of Magnesium (details in the text)[a]

| cofactor | $\Delta H_1$ (kcal/mol) | $\Delta S_1$[b] (cal mol$^{-1}$ deg$^{-1}$) | $\Delta H_2$ (kcal/mol) | $\Delta S_2$[b] (cal mol$^{-1}$ deg$^{-1}$) | $\Delta H_3$ (kcal/mol) | $\Delta S_3$[b] (cal mol$^{-1}$ deg$^{-1}$) |
|---|---|---|---|---|---|---|
| TNP-ADP with 5 mM $MgCl_2$ | −4.7±2.2 | 1.6±0.7 | 4.8±2.2 | 27±12 | 0±1 | 2.2±1.0 |
| TNP-ADP without $MgCl_2$ | −7.8±3.5 | −5.7±3 | 41.1±18 | 141±60 | −37.9±17 | −128±55 |
| TNP-ATP with 5 mM $MgCl_2$ | −6.2±2.7 | −5±2.1 | 2.6±1.2 | 18.6±7 | 4.4±2.0 | 17.5±7.3 |
| TNP-ATP without $MgCl_2$ | 0±3 | 23±10 | 22.8±10 7 | 8±30 | −2±0.8 | −4.9±2.5 |

[a] Errors are standard deviations determined using three or four independent experiments.

[b] Calculated using the binding constant determined at 10 °C.